AGU ADVANCING EARTH AND SPACE SCIENCES

Water Resources Research

RESEARCH ARTICLE
10.1029/2023WR036077

Hydrology Outweighs Temperature in Driving Production and Export of Dissolved Carbon in a Snowy Mountain Catchment

Devon Kerins[1], Kayalvizhi Sadayappan[1], Wei Zhi[1], Pamela L. Sullivan[2], Kenneth H. Williams[3,4], Rosemary W. H. Carroll[5], Holly R. Barnard[6], Matthias Sprenger[3], Wenming Dong[3], Julia Perdrial[7], and Li Li[1]

[1]Department of Civil and Environmental Engineering, The Pennsylvania State University, University Park, PA, USA, [2]College of Earth Ocean and Atmospheric Sciences, Oregon State University, Corvallis, OR, USA, [3]Lawrence Berkeley National Laboratory, Berkeley, CA, USA, [4]Rocky Mountain Biological Laboratory, Gothic, CO, USA, [5]Desert Research Institute, Reno, NV, USA, [6]Department of Geography, Institute of Arctic and Alpine Research, University of Colorado, Boulder, CO, USA, [7]Department of Geology, University of Vermont, Burlington, VT, USA

Abstract Terrestrial production and export of dissolved organic and inorganic carbon (DOC and DIC) to streams depends on water flow and biogeochemical processes in and beneath soils. Yet, understanding of these processes in a rapidly changing climate is limited. Using the watershed-scale reactive-transport model BioRT-HBV and stream data from a snow-dominated catchment in the Rockies, we show deeper groundwater flow averaged about 20% of annual discharge, rising to ~35% in drier years. DOC and DIC production and export peaked during snowmelt and wet years, driven more by hydrology than temperature. DOC was primarily produced in shallow soils (1.94 ± 1.45 gC/m^2/year), stored via sorption, and flushed out during snowmelt. Some DOC was recharged to and further consumed in the deeper subsurface via respiration (−0.27 ± 0.02 gC/m^2/year), therefore reducing concentrations in deeper groundwater and stream DOC concentrations at low discharge. Consequently, DOC was primarily exported from the shallow zone (1.62 ± 0.96 gC/m^2/year, compared to 0.12 ± 0.02 gC/m^2/year from the deeper zone). DIC was produced in both zones but at higher rates in shallow soils (1.34 ± 1.00 gC/m^2/year) than in the deep subsurface (0.36 ± 0.02 gC/m^2/year). Deep respiration elevated DIC concentrations in the deep zone and stream DIC concentrations at low discharge. In other words, deep respiration is responsible for the commonly-observed increasing DOC concentrations (flushing) and decreasing DIC concentrations (dilution) with increasing discharge. DIC export from the shallow zone was ~66% of annual export but can drop to ~53% in drier years. Numerical experiments suggest lower carbon production and export in a warmer, drier future, and a higher proportion from deeper flow and respiration processes. These results underscore the often-overlooked but growing importance of deeper processes in a warming climate.

Key Points:

- The timing, duration, and size of snowmelt is more influential than temperature in regulating the production and export of dissolved carbon
- The shallow soil zone produces and exports most of the dissolved carbon, primarily driven by snowmelt hydrology rather than temperature
- The deep zone, on average, produces 14 ± 8% and exports 27 ± 8% of dissolved carbon (DOC & DIC) and becomes more important (36 ± 2% of export) in warmer, drier years

Supporting Information:

Supporting Information may be found in the online version of this article.

Correspondence to:

D. Kerins and L. Li,
dmk6015@psu.edu;
lili@engr.psu.edu

Citation:

Kerins, D., Sadayappan, K., Zhi, W., Sullivan, P. L., Williams, K. H., Carroll, R. W. H., et al. (2024). Hydrology outweighs temperature in driving production and export of dissolved carbon in a snowy mountain catchment. *Water Resources Research*, *60*, e2023WR036077. https://doi.org/10.1029/2023WR036077

Received 15 AUG 2023
Accepted 26 JUN 2024

Author Contributions:

Conceptualization: Devon Kerins, Pamela L. Sullivan, Li Li
Data curation: Rosemary W. H. Carroll, Wenming Dong
Formal analysis: Devon Kerins
Funding acquisition: Pamela L. Sullivan, Kenneth H. Williams, Holly R. Barnard, Li Li
Methodology: Devon Kerins, Kayalvizhi Sadayappan, Wei Zhi
Project administration: Pamela L. Sullivan, Holly R. Barnard, Li Li

1. Introduction

Mountain areas cover 25% of the Earth's land surface and supply water to over 1.6 billion people globally (Meybeck et al., 2001), including 60 million in the Rocky Mountain region (Bales et al., 2006; Pfister et al., 2017). Headwater mountainous streams also contribute over 1/3rd of global stream CO_2 degassing (Marx et al., 2017), equivalent to ~16% of the annual global land carbon sink (Le Quéré et al., 2018; Raymond et al., 2013). Mountain catchments are warming at comparatively higher rates than lower lying areas, inducing higher temperature, lower discharge, and drought conditions (Overpeck & Udall, 2020; Pepin et al., 2015; Zhang et al., 2021). While these hydrologic shifts are well recognized, their impacts on terrestrial carbon transformation and lateral export, stream chemistry, and water quality have received limited attention (Bales et al., 2006; Li et al., 2022, 2024; van Vliet et al., 2023). Understanding these impacts is vital for predicting the future of carbon cycling and water chemistry, both of which are essential for preserving mountain water resources.

Terrestrial carbon fluxes have mostly been quantified by measuring vertical fluxes of CO_2 to the atmosphere, often used as the equivalent of soil respiration rates (Hashimoto et al., 2015; Kaye et al., 2005; Warner et al., 2019). Recent studies have suggested this could underestimate terrestrial carbon export by not counting carbon export via lateral groundwater fluxes carrying dissolved organic and inorganic carbon (DOC and DIC) (Duvert et al., 2018; Wen et al., 2022). In addition, dissolved carbon is an important water quality indicator. DOC

Software: Kayalvizhi Sadayappan, Wei Zhi
Supervision: Li Li
Visualization: Devon Kerins
Writing – original draft: Devon Kerins
Writing – review & editing: Kayalvizhi Sadayappan, Wei Zhi, Pamela L. Sullivan, Kenneth H. Williams, Rosemary W. H. Carroll, Holly R. Barnard, Matthias Sprenger, Julia Perdrial, Li Li

is often defined as the organic carbon fraction that passes through a 0.45 μm filter and originates from sources such as leaching, root exudates, and organic matter degradation and oxidation. DOC can form metal-DOC complexes and enhance metal mobility. It can also form carcinogenic disinfection byproducts during water treatment (Sadiq & Rodriguez, 2004; Zhao et al., 2007), causing water quality concerns particularly during spring freshets at the peak of DOC concentrations (Leonard et al., 2022). DOC can be further oxidized and become CO_2 or DIC along its flow path, often elevating stream CO_2 evasion (Grandi & Bertuzzo, 2022). DIC, often the most abundant form of dissolved carbon (Marx et al., 2017), can originate from both respiration (e.g., autotrophic root and heterotrophic respiration) and chemical weathering (Stolze et al., 2023).

Terrestrially derived DOC and DIC concentrations are closely linked to subsurface structure, flow paths, and processes (Duvert et al., 2018; Hotchkiss et al., 2015; Liu et al., 2022). DOC and DIC concentration-discharge (C-Q) relationships reveal insights into flow path contribution and solute generating processes at different subsurface depths (Botter et al., 2020). The typical C-Q pattern for dissolved carbon shows low discharge associated with the dominant delivery of DIC-rich but DOC-poor older deep groundwater (Stewart, Shanley, et al., 2022; Torres & Baronas, 2021), while high discharge is associated with greater contribution from DOC-rich but DIC-poor younger shallow soil water (Boyer et al., 1997; Burns et al., 2016; Zarnetske et al., 2018; Zhi et al., 2019).

A warmer and drier climate is likely to alter dissolved carbon (Crawford et al., 2019; Zhi et al., 2020), as temperature, snow cover, and water content simultaneously alter its production and export (Brooks et al., 2011; Kerins & Li, 2023). Soil respiration rates often increase with temperature but peak at some intermediate soil moisture (e.g., 50%–70%, (Yan et al., 2018)). During snowmelt, shallow soil water flow paths often predominate due to higher hydraulic conductivity in saturated soils (Boyer et al., 2000; Raymond & Saiers, 2010). Wet conditions enhance lateral export of dissolved, recharge of shallow soil water to the deeper subsurface, and can promote respiration rates (Clow & Mast, 2010; Wen et al., 2021). Under low flow conditions, shallow soil water wanes, deep groundwater flow becomes dominant, and vertical CO_2 effluxes to the atmosphere increase (Sullivan et al., 2019; Wen et al., 2020). Although high temperatures generally promote respiration, dry conditions can inhibit these reactions. The complex relationship between climate variables and carbon responses makes the direction and magnitude of these responses highly uncertain, challenging the quantification of riverine carbon export and regional and global carbon cycles (Duvert et al., 2018; Kirschbaum, 2006; Reynolds et al., 2017).

Existing literature has primarily focused on respiration in shallow soils. Recent studies however have shown clear evidence that deep carbon cycling beneath soils is important and cannot be overlooked in the global carbon budget (Harper & Tibbett, 2013). Organic carbon in the deep subsurface (e.g., approximately >1–2 m below the surface) is now being recognized as potentially labile (Barnes et al., 2018; Kleber & Johnson, 2010; Rumpel & Kögel-Knabner, 2011; Wan et al., 2018). Carbon respiration within bedrock fractures has been shown to exhibit rates comparable to those observed in soils (Hasenmueller et al., 2017; Tune et al., 2020). Deep respiration beneath soils have been shown to contribute to 40% of DIC production and >80% of DIC export (Stewart et al., 2024), and >7% of DIC production and >35% of DIC export (Wen et al., 2024). These deep processes however are typically not considered or quantified in Earth System models (Harper & Tibbett, 2013). There is generally a lack of process-based understanding of dissolved carbon dynamics in both the shallow soils and deep subsurface, such that it remains highly uncertain how and how much deep respiration contributes to the production and export of dissolved carbon.

Dissolved carbon concentrations reflect the intertwined processes that are sensitive to both changing flow paths and biogeochemical conditions. A warming climate can alter the proportion of the shallow and deep flow and biogeochemical reaction rates, complicating our understanding on carbon production and export. These processes and conditions however are typically studied separately within disciplinary boundaries without integration (Brookfield et al., 2021; Grimm et al., 2003; Tank et al., 2018). In addition, stream flow and chemistry data have been explored mostly via CQ relationship data analysis and statistical correlations instead of mechanistic approaches. Here we use a watershed-scale reactive transport model to integrate these processes and ask the questions: *1) What are the predominant drivers of dissolved carbon (DOC and DIC) production and export in rapidly warming, snow-dominated montane catchments? 2) How much dissolved carbon is produced and exported via the shallow and deep subsurface at daily and annual scales?* We answer these questions by using daily to weekly stream flow and dissolved carbon data from Coal Creek, a high elevation, snow-dominated catchment in the Rocky Mountains to constrain and explore the reactive transport model. We aim to offer an

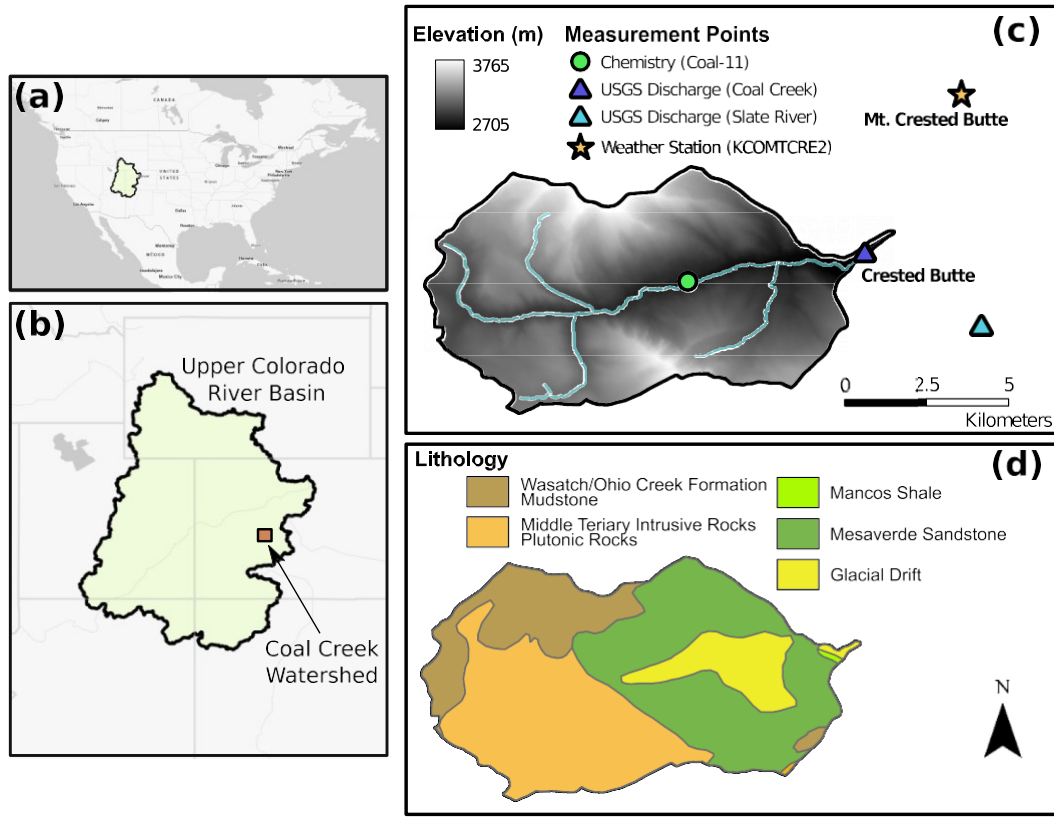

Figure 1. Coal Creek in Gunnison County, Colorado in (a) the western United Sates; in (b) the east of the Upper Colorado River Basin. (c) The 53 km^2 catchment spans an elevation gradient of 2,705 m at the mouth of the catchment to 3,765 m at its ridge, leading to a 16° average slope. (d) The dominant underlying lithology types are sandstone (39%), followed by plutonic rock (36%), and mudstone (15%).

integrated, mechanistic understanding of dissolved carbon processes and project how these dynamics may evolve in a warming climate.

2. The Study Site

The research catchment, Coal Creek (~53 km^2), is located in the traditional lands of the Núu-agha-tuvu-pu (Ute) peoples in Gunnison County, Colorado within the Upper Colorado River Basin in the Central Rocky Mountains (38°51′51.2″ N 107°02′47.3″ W) (Figure 1). The catchment elevation ranges from approximately 2,700–3,700 m with an average slope of 16°. Coal Creek is a third order stream that connects to the Slate River, which subsequently joins the East River. It is an experimental catchment of the U.S. Department of Energy supported East River Watershed Function Science Focus Area (SFA) (Hubbard et al., 2018; Kakalia et al., 2021).

The mean annual minimum and maximum daily temperatures, calculated from 1981 to 2019, are −1.5 and 9.0°C, respectively, with an overall annual average temperature around 0.9°C. The mean annual temperature (MAT) has increased about 2°C since 1980, more than a degree greater than the average increase for the United States (Zhi et al., 2020). The mean annual precipitation (MAP) is 850 mm with ~60% falling as snow (Jiang et al., 2023; Thornton et al., 2021), similar to the MAP of 973 ± 226 mm with 62 ± 6.1% falling as snow during WY2016-2021. The catchment is classified as warm summer and humid continental climate (Peel et al., 2007) and is seasonally snow-covered. Snowpack starts to accumulate in November and usually peaks in April, after which snowmelt starts.

The land-cover is dominantly evergreen forest (61%), followed by herbaceous vegetation (20%), and a small but notable presence of deciduous forest (9%), barren land (3%), and woody wetland (3%). The catchment is underlain primarily by Mesa Verde-sandstone (39% of catchment area), which dominates the eastern half of the catchment.

The western half of the north facing slope is dominated by granitic (20%) and other plutonic lithology (16%). The remainder is mostly mudstone and glacial drift. The dominant soil type is the Needleton-Scout series (49%) (SSURGO, 2023), which consist of deep, well drained soils that formed in stony and cobbly slope alluvium and colluvium. Its clay content is about 26%–32% (SSURGO, 2023). The acidity of the soil horizons range from moderate to strongly acidic (National Cooperative Soil Survey; U.S. Geological Survey, 2019).

3. Methods

3.1. Climate Data

The temperature data were from the Parameter-elevation Regressions on Independent Slopes Model (PRISM; https://prism.oregonstate.edu/) (PRISM Climate Group, 2021). The model provides daily, spatially continuous climate data for the contiguous United States. Area-normalized precipitation data were from the US Geological Survey (USGS) Precipitation Runoff System (PRMS; (Markstrom et al., 2015)) based on PRISM data for rain and Airborne Snow Observatory (ASO) data for snow distribution and snow water equivalent (SWE) (Carroll et al., 2020, 2022; Fang et al., 2019). Snow water equivalent (SWE) data were from the US Department of Agriculture (USDA) Snow Telemetry (SNOTEL) database (https://www.nrcs.usda.gov/wps/portal/wcc/home/) at Crested Butte (#380), about 5 km east of Coal Creek.

The potential evapotranspiration (PET) data were from the Environmental System Science Data Infrastructure for a Virtual Ecosystem (ESS-DIVE) (Newcomer & Rogers, 2020), (https://data.ess-dive.lbl.gov/view/doi:10.15485/1734790). PET data were available for the calendar years 2011–2020 for the East River catchment directly east of Coal Creek. Additional PET data for January–October 2021 were calculated using the Penman-Monteith equation (Monteith, 1965). The meteorologic data for PET calculations were obtained from the same WeatherUnderground source as Newcomer and Rogers (2020) (https://www.wunderground.com/dashboard/pws/KCOMTCRE2), using a Python data scraper (https://github.com/Karlheinzniebuhr/the-weather-scraper).

3.2. Water and Water Chemistry Data

Daily stream discharge data were from the USGS Water Data for the Nation: Web Interface for Coal Creek from 1 October 2014, to 30 September 2021 (Site ID: 09111250; https://waterdata.usgs.gov/usa/nwis). Stream discharge was collected during ice-free periods, generally ranging from 1 April to 15 November each year. Because discharge measurements could not be recorded at Site 09111250 during periods of ice cover, a regression equation developed using the downstream Slate River USGS site (Site ID: 385106106571000) was used to infill data gaps from November to April ice-covered time.

Stream chemistry has been measured for >40 solutes since 2016 (Dong et al., 2024; Zhi et al., 2019). From April through October, stream samples were taken by an automatic water sampler (Model 3700; Teledyne ISCO, NE, USA) at Coal-11 (Figure 1) every other day; from November through March, samples were taken by a grab-sample once a week. Details of sampling and measurements are discussed in Text S1 in Supporting Information S1. For this work we focus on DOC and DIC measurements.

3.3. Hydrology Model—Hydrologiska Byråns Vattenaydelnig (HBV) Model

We used the widely applied hydrology model HBV (named after *Hydrologiska Byråns Vattenavdelnig*) (Bergström, 1976; Seibert & Vis, 2012). The model simulates major processes including snow accumulation and melting, soil moisture, and runoff response (including groundwater). The model used a degree day approach to calculate snowmelt rates and partitions snowmelt and precipitation input between evapotranspiration (ET) and discharge based on water and energy balance. It conceptualizes the catchment as two stacked upper and lower buckets defining two subsurface zones (Figure 2), which further partitions discharge into three different flows: the quick flow Q_0 that we conceptualize as surface flow (Q_{SF}), intermediate flow Q_1 that we conceptualize as flow from the shallow soil zone (Q_{SZ}), and slow flow Q_2 that is considered as flow from deep zones (Q_{DZ}). Quick flow occurs when the SZ storage exceeds a limit.

By doing so, the model assesses the temporal dynamics and average behavior of the entire catchment without an explicit landscape representation. Although the model does not explicitly delineate a vadose and saturated zone, the SZ is mostly unsaturated, except during times of high flow, and can be considered as predominately vadose, whereas the deeper zone is more regularly saturated.

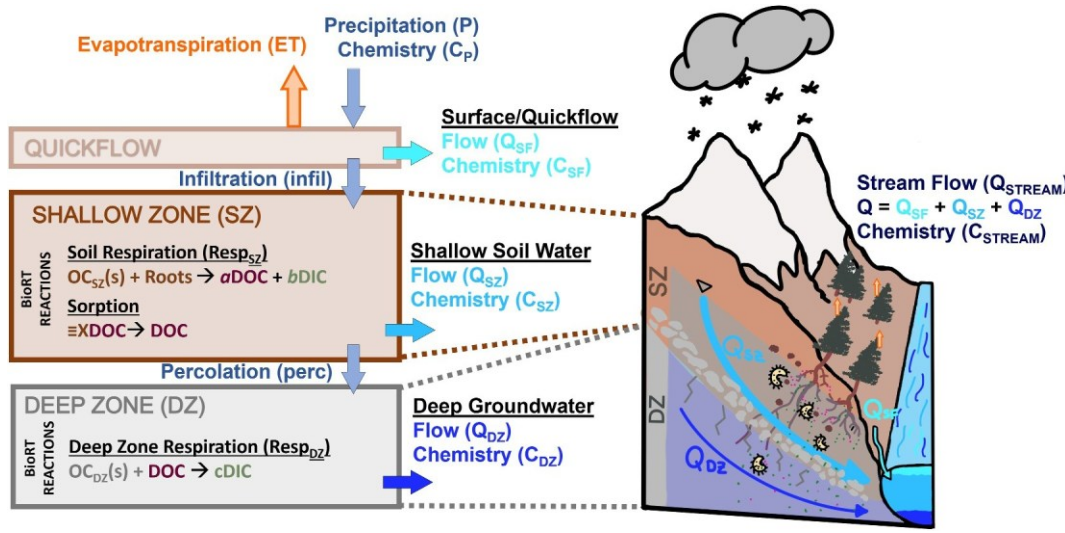

Figure 2. BioRT-HBV Conceptual Figure. Stream flow comes from three distinct flow paths, Quick flow (Q_{SF}, or Q_0 in HBV terminology) which typically occurs above or near the ground surface, intermediate flow from the shallow zone (SZ) that conceptually represents soil zone interflow (Q_{SZ}, or Q_1 in HBV terminology), and flow from the deep zone (DZ) that represents deeper and longer flow paths (Q_{DZ}, or Q_2 in HBV terminology). Users can define reaction networks for their own purposes. In this work, BioRT-HBV simulates soil respiration ($Resp_{SZ}$) and sorption in the SZ, and deep zone respiration ($Resp_{DZ}$) or the further degradation of organic carbon that occurs in slower and longer flow paths. These key reactions and their calibrated parameters are detailed in Table 1.

The model uses time series (daily) of air temperature, precipitation, and potential evapotranspiration as input. Model output includes time series of ET, the different Qs, and water storage in each zone. The calculated water storage in each zone represents the "dynamic" storage, or the water storage that responds and contributes to streamflow (Soulsby et al., 2011). The "passive" water storage that supports vegetation, solute transport, and biogeochemical reactions typically cannot be differentiated using only hydrometeorological observations (Kirchner, 2009), and is thus determined during reactive transport model calibration.

3.4. Reactive Transport Model—BioRT-HBV

BioRT-HBV inherits the reactions and setup of the BioRT module in BioRT-Flux-PIHM (Zhi et al., 2022) but uses hydrologic outputs (water storage and flow components) from HBV as input (Sadayappan et al., 2024a). It therefore follows the conceptual structure of HBV and simulates biogeochemical reactions and solute transport at the catchment scale. The model solves mass conservation equations for dissolved solutes, considering solute transport, and abiotic and biogeochemical reactions. BioRT simulates kinetically controlled reactions including chemical weathering that follows Transition State Theory (TST) rate law, and microbe-mediated reactions that borrow dual-substrate Monod kinetics with inhibition terms (Li, 2019; Monod, 1949) when there are dependencies on substrates and microbial abundance. The model also simulates fast, thermodynamically controlled reactions such as ion exchange, surface complexation, and aqueous complexation.

Below we show representative mass conservation equations using DOC as an example solute. We skipped the equation for the surface zone (SF) as the fraction of SF is negligible (detailed later) and we assume no reactions in SF for DOC and DIC in this work.

In Shallow Zone (SZ):

$$\frac{d(V_{w,SZ}C_{SZ,DOC})}{dt} = Q_{Infil}C_{infil,DOC} + R_{SZ,DOC} - Q_{SZ}C_{SZ,DOC} - Q_{Perc}C_{SZ,DOC} \quad (1)$$

In Deep Zone (DZ):

Table 1
*Key Reactions and Calibrated Parameters *the Models Were Calibrated Separately for Years With Average DOC Concentrations and High DOC Concentrations (Italicized Text in Parathesis)*

	Shallow soil zone (SZ) respiration ($Resp_{SZ}$) *Reaction 1*	Deep zone (DZ) respiration ($Resp_{DZ}$) *Reaction 2*	Sorption ($Sorp_{SZ}$) *Reaction 3*
Reaction Equation	$OC_{SZ}(s) + Roots \rightarrow \mathbf{a}DOC + \mathbf{b}DIC$	$OC_{DZ}(s) + DOC \rightarrow \mathbf{c}DIC$	$\equiv XDOC \leftrightarrow DOC$
Stoichiometric Coefficients	$\mathbf{a}$ = 0.16 *(0.16)*	$\mathbf{c}$ = 1.3 *(0.85)*	–
	$\mathbf{b}$ = 0.11 *(0.20)*		
Rate Law $r = \log_{10}$ Keq	$kAf(Z_w)f(T)f(S_w)$	$kAf(Z_w)f(S_w)$	$kA(1 - \frac{C_{DOC}}{K_{eq}})\,f(T)\,f(S_w)$
	–	–	−3.36 *(−3.26)*
$\log_{10}k$ – (mol/m²/s)	−7.05 *(−7.05)*	−12.0 *(−12.0)*	−6.53 *(−6.53)*
SSA[a] – (m²/g)	0.108 *(1.8E−3)*	0.029 *(0.048)*	1.5E−4 *(1.5E−4)*
$_{10}$	2.10 *(1.10)*	1.00 *(1.00)*	1.14 *(1.14)*
$f(S_w)$ – n[c]	2.94 *(2.94)*	2.50 *(2.21)*	0.99 *(0.99)*
$f(S_w)$ – $S_{w,c}$[d]	0.87 *(0.87)*	1.00 *(1.00)*	1.00 *(1.00)*
$f(Z_w)$ – n1 × Sα[e]	0.003 *(0.001)*	0.0001 *(0)*	0 *(0)*
Passive Storage (mm)	**SZ**: 77.4s	**DZ**: 300.0	

[a]SSA is specific surface area, which is used to calculate the surface area with OC volume fraction and density in the model. [b]The calibrated values of Q_{10} for Rxn 1 ($Resp_{SZ}$) for the shallow soils is around reported values of ∼2 for forested catchments at similar altitude (Zeng et al., 2022). The Q_{10} for Rxn 2 ($Resp_{DZ}$) is set at 1.00 for the reactions at depth (no dependence on T). The calibrated $Q_{10\ for}$ Rxn 3 ($Sorp_{SZ}$) is within the range of reported values (Conant et al., 2011). [c]The exponent for the soil moisture dependence function reflects the effect of soil water content on reactions and typically ranges from 1.2–3.0 (Hamamoto et al., 2010). [d]$S_{w,c}$ at which $f(S_w)$ reaches its maximum, typically at intermediate soil moisture (e.g., 50%–70%) and the extent of dependence on soil moisture n (Yan et al., 2018). [e]"0" means no dependence on water table depth.

$$\frac{d(V_{w,DZ}C_{DZ,DOC})}{dt} = Q_{Perc}\,C_{SZ,DOC} + R_{DZ,DOC} - Q_{DZ}\,C_{DZ,DOC} \quad (2)$$

In Stream mixing:

$$C_{STREAM,DOC}(t) = \frac{Q_{SF}(t)\,C_{SF,DOC}(t) + Q_{SZ}(t)\,C_{SZ,DOC}(t) + Q_{DZ}(t)\,C_{DZ,DOC}(t)}{Q_{SF}(t) + Q_{SZ}(t) + Q_{DZ}(t)} \quad (3)$$

Here Q_{Infil} is infiltration flow from surface to shallow zone [mm/d]; Q_{Perc} is percolation flow from shallow zone to deep zone, or recharge [mm/d]; and $V_{w,SZ/DZ}$ is the water storage in SZ or DZ normalized to catchment area [mm]; $C_{SZ/DZ,DOC}$ is the concentration of DOC in SZ or DZ [mol/L]; $Q_{SF/SZ/DZ}$ is the flow rate from SF, SZ, or DZ normalized to catchment area [mm/d]; and $r_{SZ/DZ,DOC}$ is the reaction rate of DOC in SZ or DZ [mol/m²/d]. The water from different zones (SF, SZ, and DZ) mix in streams. The proportions of different flows and their respective chemistry determine stream concentrations. Without reactions in SF, the concentrations in SF are the concentrations in precipitation divided by the runoff ratio (Q/P) to reflect the concentrating effect of the evapotranspiration process. The governing equations are the same for DIC, although their reaction terms may be different, as we detail in Table 1.

The model solves these equations and generates modeled reaction rates and concentrations (C) of dissolved solutes in the surface, shallow, and deep subsurface zones (C_{SF}, C_{SZ}, & C_{DZ}) and the stream (C_{STREAM}). These quantities reflect the average, effective response of the entire catchment. The BioRT model is calibrated against a time series of stream carbon concentration data, as we detail in the next section.

3.5. Biogeochemical Reactions and Rate Laws

Taking a parsimonious approach, we set up reactions that are essential to reproduce the dynamics of DOC and DIC observations, such that we can limit the number of calibration parameters. DOC and DIC are generated primarily from biological processes in Coal Creek. In heterotrophic respiration, microbes decompose organic

matter into DOC and CO_2—contributing to DIC—as DIC is the sum of CO_2(aq), CO_3^{2-}, and HCO_3^- that speciate rapidly in water and can quickly transform from one species to another. Exchange between dissolved and gaseous carbon forms also occur relatively fast. During autotrophic respiration, plant roots produce CO_2, adding to DIC. Roots also produce DOC as root exudates. The relative contributions from heterotrophic and autotrophic respiration are difficult to quantify and can change over time and space. We therefore lumped them as soil "respiration" ($Resp_{SZ}$, Reaction 1, Table 1) (Barba et al., 2018; Hanson et al., 2000). $Resp_{DZ}$ (Reaction 2, Table 1) represents respiration in the DZ from sources such as translocated DOC (from SZ), petrogenic carbon (Dean, 2019; Soulet et al., 2018), and deep root exudates (OC_{DZ}). It also lumps in the direct input of DIC from deep root respiration, if present (Tune et al., 2020). The rates of these reactions that involve DOC in SZ and DZ are R_{SZ} and R_{DZ} terms in Equations 1 and 2.

The term "OC" broadly represents organic carbon that typically consists of a variety of compounds. We do not have data to differentiate the contribution of heterotrophic and autotrophic pathways or the relative amount of consumption versus production such that we lumped these processes, a common practice when the goal is to quantify the effective reaction rates (Davidson & Janssens, 2006). We do not explicitly include the respiration of DOC to produce DIC. Rather it is considered as part of a "net" reaction where both OC and DOC can generate DIC and DOC is an intermediate product that is not always fully oxidized to DIC. The concentration of DOC therefore reflects the balance between reactions that produce and consume DOC, in addition to transport. DOC can also sorb onto soil surfaces depending on the sorption affinity and available sorption sites ("≡X" in Reaction 3, in Table 1), which can be either DOC desorption from ($Desorp_{SZ}$) or adsorption ($Adsorp_{SZ}$) to soils.

OC is assumed to be abundant such that the reactions depend on temperature (T), soil water content (Sw), and water table depth (Zw):

$$r_{bio} = kAf(T)f(S_w)f(Z_w) \tag{4}$$

Where r_{bio} = biologically mediated reaction rate [mol/d]; k = kinetic reaction rate constant [mol/m^2/d]; and A = effective contact area among reactants (electron donor and acceptors) per unit volume of soil [m^2/L]. In the more anoxic DZ with limited oxygen, other electron acceptors (i.e., Fe-oxides, nitrate, & sulfate) and DOC transported to the DZ can support slower deep respiration. With slower moving water and longer residence times, DZ respiration may decompose more humic substances that are often more abundant at depth in montane systems (Keller, 2019; Marin-Spiotta et al., 2009).

For sorption (Reaction 3, in Table 1), $\equiv XDOC$ represents DOC sorbed to soil surface sites. As explained later in the calibration section, sorption is simulated kinetically to capture the DOC dynamics:

$$r_{sorption} = kA\left(1 - \frac{C_{DOC}}{K_{eq}}\right)f(T)f(S_w) \tag{5}$$

The "solubility" of DOC in the aqueous phase, or K_{eq}, represents the limit of how much DOC can be in water before sorbing to soil surfaces. Larger K_{eq} values indicate higher maximum DOC in water. When $C_{DOC} > K_{eq}$, DOC sorbs on soil surfaces, when $C_{DOC} < K_{eq}$, DOC desorbs from soil surfaces. Surface area A (m^2) is the surface area of the soil materials, calculated based on specific surface area (SSA, m^2/g), volume fraction (m^3/m^3), and solid density (g/cm^3).

The temperature dependence function ($f(T)$) follows the extensively used Q_{10} form (Lloyd & Taylor, 1994):

$$f(T) = Q_{10}^{\frac{T-20}{10}} \tag{6}$$

where values of Q_{10} represent the relative increase in reaction rates when temperatures increase by 10°C. The soil moisture dependence function ($f(S_w)$) includes the critical soil moisture ($S_{w,c}$) at which $f(S_w)$ reaches its maximum, typically at intermediate soil moisture (e.g., 50%–70%), and the extent of reaction rate dependence on soil moisture (n) (Yan et al., 2018):

$$f(S_w) = \begin{cases} \left(\frac{S_w}{S_{w,c}}\right)^n, & S_w < S_{w,c} \\ \left(\frac{1 - S_w}{1 - S_{w,c}}\right)^n, & S_w > S_{w,c} \end{cases} \quad (7)$$

When soil moisture is below $S_{w,c}$, $f(S_w)$ increases with soil moisture; when soil moisture is above $S_{w,c}$, $f(S_w)$ decreases with soil moisture representing, for example, a decrease in reaction rates due to limited O_2 under more saturated conditions. The depth dependence function $f(Z_w)$ is as follows (Seibert et al., 2009; Weiler & McDonnell, 2006):

$$f(Z_w) = \exp(-\alpha {Z_w}^{n1}) \quad (8)$$

The depth dependence parameter (α) determines how fast $f(Z_w)$ changes with water table depth and the direction parameter ($n1$) determines if $f(Z_w)$ will increase or decrease with water table depth. The depth dependence function is important to represent the dependence of reaction rates on rising and falling water tables.

3.6. Model Calibration

3.6.1. Hydrology Calibration

The stream discharge time series data was split into training and testing periods for calibration. The training period used data in water years (WY, October.1–September.30) 2017–2020 and the testing period used data in WY 2016 and 2021. The 2014 water year was used as a spin-up period. The data splitting allowed the model to train on two representative low flow and two high flow years. Hydrology was initially calibrated by running 5 million Monte Carlo simulations with parameters within ranges previously used for a global scale study (Beck et al., 2016). Model performance was assessed based on three metrics: the Nash-Sutcliffe Efficiency (NSE) to assess fit on peak flows, NSElog to assess fit on low flows, and percent bias (PBIAS) to assess overall volume. Of the 5 million Monte Carlo simulations, 340 cases had a "great" fit for the training period (NSE > 0.75, NSElog > 0.75, & |PBIAS| < 10%) and at least a "good" fit for the testing period (NSE > 0.5, NSElog > 0.5, |PBIAS| < 20%) (Figure S1 in Supporting Information S1; Texts S2 and S3, Figures S1–S3 in Supporting Information S1). Hydrology cases were further tuned iteratively after considering biogeochemical reactions and comparing with time series data of stream DOC and DIC concentrations. In other words, stream chemistry data were additionally used to narrow down the hydrology and flow path partitioning.

3.6.2. Biogeochemistry Calibration

The reaction network was implemented by adding one reaction at a time, starting from shallow zone soil respiration ($Resp_{SZ}$). This approach helps evaluate the effects of individual processes on stream chemistry and their interaction. We do not explicitly track other solutes, which necessitates more complex rate laws with unconstrained reaction parameters. Reaction parameters and passive water storage were manually calibrated using a priori knowledge and trial and error (Table 1). The best fit was determined by NSE and KGE for reproducing stream DOC and DIC data.

In the respiration reactions, the relative carbon transformation to DOC and DIC is represented by the reaction stoichiometry coefficients (a, b, and c; Table 1). These "effective" reaction stoichiometries represent the average magnitude of OC transformation to DOC and DIC at the catchment scale, which depend on wide-ranging factors including flow paths, vegetation, soil water pH, and temperature (Roth et al., 2015; Zhou et al., 2023). The rates of the three reactions follow the reaction rate laws and sensitivities in Equations 4–8. The reaction stoichiometry and rate parameters were calibrated (Table 1).

Even with a slim reaction network (three reactions), the complexity of reaction stoichiometry and rate laws leads to many parameters. This is common in reactive transport modeling, as the reaction thermodynamics and kinetics include many parameters. See for example, in Maher et al. (2006), Zhi et al. (2019), Wen et al. (2020), Xu et al. (2022), and Stolze et al. (2023). One might expect this would lead to substantial equifinality issue with many cases fitting data. However, our experience in calibrating reactive transport models is the opposite. When we set up millions of BioRT runs with widely ranging parameter values, we did not have simulation cases that reproduce

stream carbon data. BioRT almost always needs to be manually calibrated with modelers' knowledge on how flow and reactions are expected to change solute concentrations. This may be unexpected as it is not the case for example, in HBV calibrations, millions of simulations can lead to hundreds of cases that reproduce stream flow data. We do not yet understand this stark difference in equifinality in hydrology and biogeochemical calibration. We speculate this may be due to the high interdependence between solute concentrations via multiple reactions with non-linear kinetics and thermodynamics such that only a very small parameter space can reproduce observations.

The sorption reaction (Reaction 3, Table 1) was initially considered as an equilibrium-controlled reaction that represents the rapid approach to sorption limits (equilibrium) and instantaneous release and sorption of DOC without the gradually changing dynamics (Neff & Asner, 2001). Such reaction characteristics however could not reproduce the simultaneous peaks of stream DOC and streamflow during snowmelt. A kinetically controlled sorption was essential to generate such dynamics, likely because it represents the gradual mobilization of sorbed DOC as snowmelt raises water table into the DOC-rich topsoil and expands to uphill slopes.

The calibration was unsuccessful in capturing the continuous 6-year time series of carbon dynamics. The notable outliers are WY 2017 and 2018 when the peak stream DOC concentrations are more than three times higher than those in other years. Therefore, two separate models were calibrated (Clark et al., 2011): One fit only to the years with typical stream DOC concentrations and one fit only to those with high stream DOC concentrations. The potential differences across different years may include, for example, soil destabilization (e.g., mining, environmental management works, recreation) in the high DOC years that can elevate DOC concentrations in WY17 and WY18. Stream DIC concentration data in all years were reproduced by both model calibration scenarios. Our analysis in results focused on model results calibrated to the typical years with average DOC concentrations.

3.7. Model Uncertainty and Sensitivity Analysis

We calibrated HBV for hydrology first and then used a representative HBV case for BioRT calibration. The acceptable HBV cases have high model performance values but span a range of hydrologic partitioning. The HBV case chosen for BioRT calibration represented the mean discharge behavior of all acceptable runs. This case was further fine-tuned based on chemistry calibration, as stream chemistry reflects source water composition and flow path partitioning. To assess the possible range of BioRT output with acceptable HBV runs, three HBV runs were selected to represent the maximum (0.41), minimum (0.06), and mean (0.19) of fraction of deeper flow ($f(Q_{DZ})$, or Q_{DZ} over Q at the annual scale) from all acceptable HBV runs. When using the minimum $f(Q_{DZ})$ case, peak DOC and overall DIC concentrations become more diluted, due to more shallow soil water than the measured data; when using the maximum $f(Q_{DZ})$ case, peak DOC and overall DIC concentrations exceed the measured data (Text S4 and Figure S4 in Supporting Information S1).

A parameter sensitivity analysis was additionally carried out for all reactions ($Resp_{SZ}$, $Resp_{DZ}$, and SorpSZ (Text S5, Figure S5 and S6 in Supporting Information S1). Parameters for $Resp_{SZ}$ tend to be the most sensitive, indicating its role as an essential "driver" compared to other reactions. Reaction rate constants and surface area are equally important for $Sorp_{SZ}$, indicating overall sorption rates are key to capture DOC dynamics. The $Resp_{SZ}$ reaction is the most important for determining sorption dynamics, indicating soil respiration drove sorption dynamics. The soil moisture parameters are the most sensitive for $Sorp_{SZ}$, while deep respiration ($Resp_{DZ}$) has negligible influence on sorption.

3.8. Catchment-Scale Export and Production Rates

The total production rates (R_P) of DOC and DIC including both SZ and DZ can be calculated as the following.

$$R_{P,\text{DOC Total}} = r_{\text{SZ,Resp}} \times a \tag{9}$$

$$R_{P,\text{DIC Total}} = r_{\text{SZ,Resp}} \times b + r_{\text{DZ,Resp}} \times c \tag{10}$$

Here r is the simulated reaction rate and a, b, & c are the calibrated stoichiometric coefficients (Table 1). Rates of solute export (R_E) were calculated as the water outfluxes times the concentrations of DOC (C_{DOC}) or DIC (C_{DIC}) in each zone (and therefore flow paths).

Table 2
Description of Cases and Climate Scenarios Used for Climate Scenario Experiments

Climate scenario	Case	Description	Q [mm/yr]	T_{AVE} [°C]	T_{MAX} [°C]
I. Sustained dry conditions	1. Dry-HighT_{MAX}	repeats WY 2021, dry year with the highest annual maximum temperature (T_{MAX})	275 (model) 189 (data)	3.0	18.6
	2. Dry-HighT_{AVE}	repeats WY 2018, dry year with the highest average annual temperature (T_{AVE});	245 (model) 213 (data)	4.1	18.1
II. Sustained wet conditions	3. Wet-LowT	repeats WY 2019	610 (model) 693 (data)	2.0	17.0
III. Alternating wet and dry conditions	**4. Wet-LowT**/ Dry-HighT_{MAX}	alternates **WY 2019** followed by WY 2021	**610**/275 (model) **693**/189 (data)	**2.0**/3.0	**17.0**/18.6
	5. Wet-LowT/ Dry-HighT_{AVE}	alternates **WY 2019** followed by WY 2018	**610**/245 (model) **693**/213 (data)	**2.0**/4.1	**17.0**/18.1

Note. Bold font in scenario III are for values used in Wet-lowT year represented by WY2019.

$$R_{E,\mathrm{DOC\ Total}} = C_{\mathrm{SF,DOC}} \times Q_{\mathrm{SF}} + C_{\mathrm{SZ,DOC}} \times Q_{\mathrm{SZ}} + C_{\mathrm{DZ,DOC}} \times Q_{\mathrm{DZ}} \quad (11)$$

$$R_{E,\mathrm{DIC\ Total}} = C_{\mathrm{SF,DIC}} \times Q_{\mathrm{SF}} + C_{\mathrm{SZ,DIC}} \times Q_{\mathrm{SZ}} + C_{\mathrm{DZ,DIC}} \times Q_{\mathrm{DZ}} \quad (12)$$

3.9. Numerical Experiments for Future Climate Scenarios

To evaluate the impacts of possible climate scenarios, the calibrated model was used to conduct numerical experiments over a 10-year period (WY 2021–WY 2031). The HBV hydrologic outputs from selected years were used as inputs for the calibrated BioRT model. We ran five cases which are categorized into three scenarios, each has different temperature and discharge combination (Table 2). The warmest and driest years, WY 2018 and WY 2021, were chosen to represent the warmer and drier conditions forecasted for the Rocky Mountain region. While WY 2019 was selected as a wetter and cooler year that is more representative of historical conditions.

Dry-HighT_{MAX} and Dry-HighT_{AVE} are similar in their mean annual discharge but differ in respect to their temperature profiles and timing of discharge. These timing differences allow us to assess the impacts of both streamflow timing and magnitude changes. Dry-HighT_{MAX} represents higher temperatures during the growing season, but snowmelt timing remains similar to historical timing. Dry-HighT_{AVE} represents higher temperatures throughout the year and thus an earlier snowmelt timing. A more arid climate can still persist even with year-to-year variations in hydrologic regime (Overpeck & Udall, 2020). Therefore, scenarios of alternating the wet and cool year and the selected dry years were conducted to account for potential year-to-year variability in more arid future climate conditions.

4. Results

4.1. Hydrology Dynamics

HBV captured the multi-year dynamics of stream flow with a high NSE value (NSE = 0.87, Figure 3, Table S1 in Supporting Information S1). Modeled values of average annual ET were 468 ± 28 mm, compared to the average annual value of 1544 ± 212 mm for PET from model input. The average aridity index (PET/P) was 1.66 ± 0.48, indicating Coal Creek as water-limited. The annual runoff ratios varied between 0.3 and 0.5 (0.41 ± 0.08). An annual average of 76 ± 10% of the stream discharge was sourced from snowmelt. Snowmelt occurred between April and July and peak snowmelt typically happened in June (Figure 3). As snowmelt started, the shallow soil water flow Q_{SZ} increased and became dominant until snowmelt receded before August, at which time Q_{SZ} decreased and Q_{DZ} became dominant. This annual hydrograph dynamic occurred similarly in each water year, although the timing, magnitude, and duration of snowpack and snowmelt varied from year to year.

The total deeper flow (Q_{DZ}) remained relatively similar across the years, yet the annual fractions of different flow components varied from year to year (Figure 3b). Dry years (low Q) showed a higher fraction of deeper flow ($f(Q_{DZ})$) and a lower fraction of shallow flow ($f(Q_{SZ})$). In contrast, wet years with more snow and snowmelt

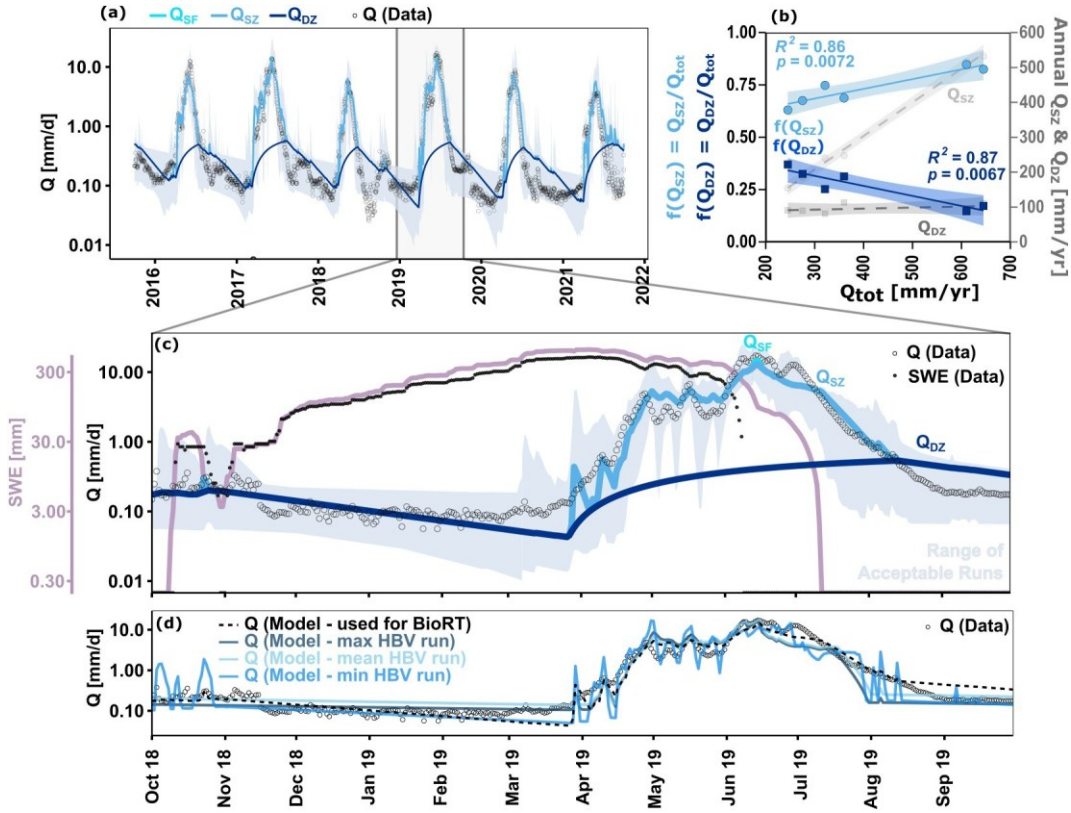

Figure 3. Time series of stream discharge showing (a) data and model output of stream discharge and flow components (Q_{SF}, Q_{SZ}, and Q_{DZ}) from HBV. The range of acceptable runs (gray shaded area) encompasses the variation of the measured stream discharge data (empty black circles). (b) Total annual flow from SZ and DZ flow paths and their fractions ($f(Q)$) over total annual stream flow. Total stream flow decreases at the expense of decreasing Q_{SZ} while Q_{DZ} remains relatively constant across years leading to increasing $f(Q_{DZ})$ in drier years. (c) Zoomed in figure for WY 2019, a higher flow year with snow water equivalent (SWE) with streamflow composed of Q_{SZ}, Q_{SF}, and Q_{DZ}. Empty black circles and lines are data and model output, respectively. (d) A range of model output from HBV cases representing the mean of all acceptable model runs, the maximum and minimum fraction of deep discharge cases, and the fine-tuned HBV case that was used for BioRT (dashed black line) compared to measured Q (empty black circles).

generally had lower $f(Q_{DZ})$ and higher $f(Q_{SZ})$, suggesting higher water fractions routing through SZ. Q_{SZ} made up about 73.5 ± 8.7% of annual stream flow, whereas the deeper Q_{DZ} made up about 26.5 ± 8.9%. The third flow component representing quick flow/surface flow (Q_{SF}) only contributed during peak snowmelt in the wettest years, WY2017 and WY2019. In WY2019, Q_{SF} contributed about 7% of annual stream flow, compared to 82% and 11% for Q_{SZ} and Q_{DZ}, respectively. In all but the wettest years (WY17 & WY 19), Q_{SZ} and Q_{DZ} made up >99% of stream flow.

Flow and subsurface storage varied substantially in the SZ and had much smaller variation in the DZ (Figure S7 in Supporting Information S1). The SZ was dominated by dynamic storage. On the other hand, the DZ had less dynamic storage and a greater amount of passive storage. Even though DZ water storage in a natural system would be significantly larger than the model output, we do not know the bottom of the aquifer and the model represents the storage in the DZ that interacts with streamflow. Overall, the majority of water in the SZ contributed to stream flow, whereas the majority of DZ water is passive and did not contribute to streamflow generation but was important for biogeochemical reactions, as discussed later.

4.2. Temporal Dynamics of Stream Carbon

The dissolved carbon concentration data showed a seasonal cycle (Figure 4). Stream DOC concentrations peaked and DIC concentrations toughed during highest snowmelt pulses in late spring and early summer (Figures 4a and 4c). DOC exhibited a flushing pattern with concentration increasing with flow and DIC displayed a dilution

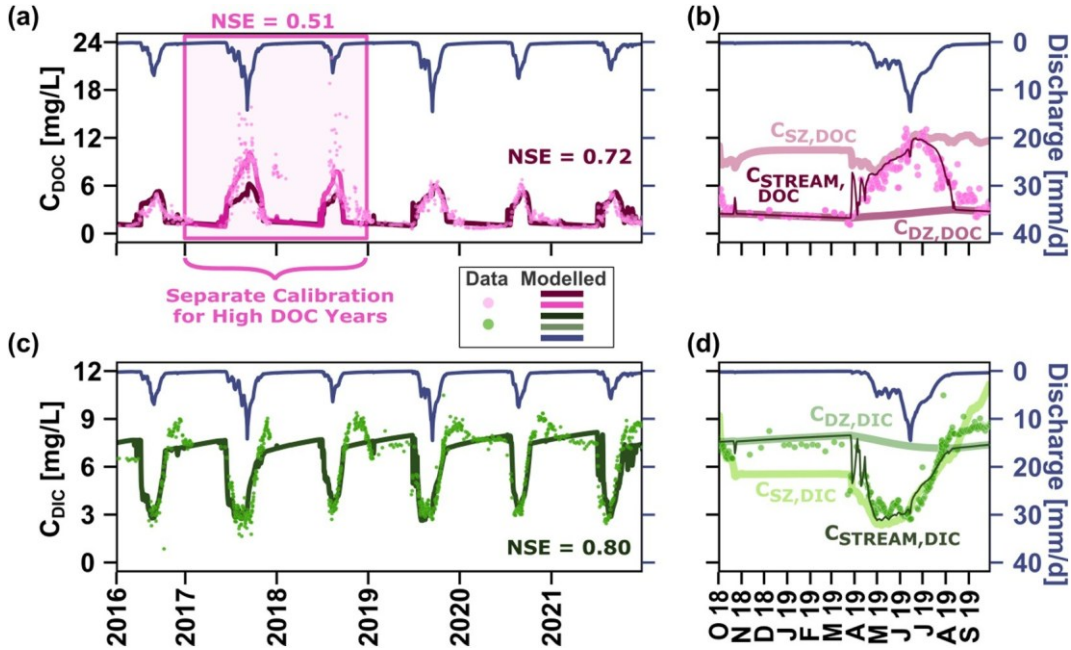

Figure 4. Timeseries of dissolved carbon (a) data and modeled stream DOC concentrations (bright pink points) from two calibrated scenarios: the average DOC concentrations (in WY 2016, 2019, 2020, & 2021; NSE_{DOC} = 0.72, KGE_{DOC} = 0.83; dark pink solid line) and the high DOC concentration (in WY 2017 & 2018; NSE_{DOC} = 0.51, KGE_{DOC} = 0.67; light line). (c) DIC was calibrated and had a similar fit for all years (NSE_{DIC} = 0.80, KGE_{DIC} = 0.80). The concentrations of (b) DOC and (d) DIC in the stream, SZ (solid line), and DZ (dashed line) in WY2019, a representative wet year. Stream concentrations, $C_{STREAM,DOC}$ and $C_{STREAM,DIC}$, are a result of mixing flow from different paths, thus fall between SZ and DZ concentrations. At low flow, $C_{STREAM,DOC} \approx C_{DZ,DOC}$ and $C_{STREAM,DIC} \approx C_{DZ,DIC}$ or stream concentrations were essentially those in the DZ. At high flow; $C_{STREAM,DOC} \approx C_{SZ,DOC}$ and $C_{STREAM,DIC} \approx C_{SZ,DIC}$, or stream concentrations are the same as those in the SZ.

pattern with concentration decreasing with flow. During the low flow in the fall and winter, $C_{STREAM,DOC}$ and $C_{STREAM,DIC}$ remained constant at about 2.4 mg/L and 7.2 mg/L, respectively. These stream concentrations reflected the respective concentrations in the DZ of $C_{DZ,DOC}$ and $C_{DZ,DIC}$ (Figures 4b and 4d), which indicated stream flow was dominated by DZ groundwater at low flow. During peak snowmelt and peak flow, $C_{STREAM,DOC}$ and $C_{STREAM,DIC}$ reflected $C_{SZ,DOC}$ and $C_{SZ,DIC}$ respectively, which indicated the dominance of SZ water in streamflow under wet conditions.

Interestingly, measured stream DIC concentrations peaked each year after the falling limb of the snowmelt driven discharge. These concentrations were higher than the majority of stream DIC concentrations during low flow in late fall and winter and were not captured by BioRT modeling output. The amount of DIC represented in this "bump" was estimated by calculating the difference between model output and the measured data during this time period, which yielded on average, 0.052 ± 0.032 g C/m^2/yr, equivalent to 2,756 kg C/yr for the entire watershed.

Stream DOC concentration typically increased steadily to peak values around 6 mg/L and decreased with streamflow (in 2016, 2019, 2020, and 2021). In 2017 and 2018, however, DOC concentrations increased rapidly to peak at around 18 mg/L, about three times higher than average, and dropped rapidly. The model could not be calibrated to capture both the typical and these disparate multiyear peak DOC dynamics; therefore, two models were calibrated (Table 1). One model was fit to the average DOC concentration. BioRT model parameters, mostly related to reaction rate controls, were then adjusted to fit the high DOC concentrations (Table 1; *italicized values*). The parameter adjustments resulted in higher reaction rates, lower sensitivity to temperature and soil moisture, and higher capacity for DOC concentrations in aqueous phase. Model performance was satisfactory in both cases (Figures 4a and 4c & Table S1 in Supporting Information S1), however, the NSE value was not as good in the high DOC case, possibly due to the large variation between 4.8 and 20.4 mg/L in the relatively short snowmelt period. Further analysis in the rest of the paper focuses on the modeling output from the typical, average DOC model case.

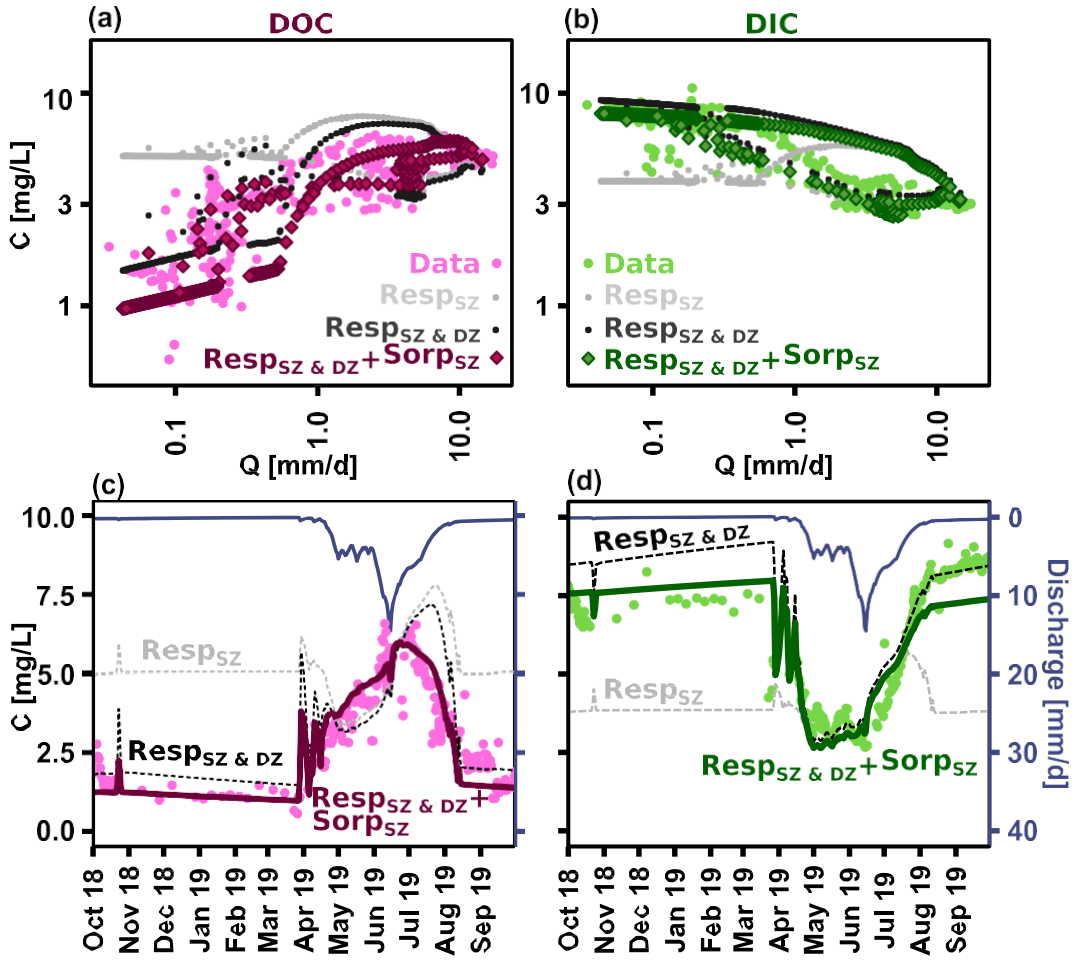

Figure 5. Concentration discharge plots (a, b) and time series (c, d) of modeled (a, c) DOC and (b, d) DIC concentrations in WY 2019, a representative wet year, in different reaction scenarios. Comparison of three scenarios ($Resp_{SZ}$ only: light gray dot and solid line, $Resp_{SZ\ \&\ DZ}$: dark gray dots and solid line, and $Resp_{SZ\ \&\ DZ}$ + $Sorp_{SZ}$: solid color dot and lines) indicate $Resp_{DZ}$ is essential for reproducing low DOC and high DIC at low flow. $Sorp_{SZ}$ of DOC acted as a buffer mechanism and was essential for capturing the DOC peak during snowmelt.

4.3. Key Reactions That Shape Stream Carbon Dynamics

The stream carbon dynamics were captured using only three reactions: $Resp_{SZ}$, $Resp_{DZ}$, and $Sorp_{SZ}$. Stepwise addition of these reactions illuminated the effects of each reaction (Figure 5). $Resp_{SZ}$ was essential in setting the baseline of $C_{SZ,DOC}$ and $C_{SZ,DIC}$, especially during snowmelt, as indicated by the difference between the calibrated case and the $Resp_{SZ}$ only scenario. However, $C_{STREAM,DOC}$ and $C_{STREAM,DIC}$ at low streamflow times were not captured with only $Resp_{SZ}$. Carbonate weathering is likely not a dominant source of DIC in the DZ, as Coal Creek is underlain by only limited calcareous shale interbeds (Gaskill et al., 1967, 1987), therefore, only $Resp_{DZ}$ was implemented in the DZ. $Resp_{DZ}$ consumed DOC recharged from the SZ and generated DIC in the DZ, therefore reducing DOC concentration but increasing DIC concentration in DZ. It turns out that $Resp_{DZ}$ was essential to reproduce the low $C_{STREAM,DOC}$ and high $C_{STREAM,DIC}$ at low streamflow when most stream water comes from DZ.

Calibrated $Resp_{DZ}$ stoichiometry revealed the relative production of DIC in the DZ from newly generated DOC from the SZ versus DZ carbon sources, such as processed and petrogenic carbon sources (variable c in Table 1; Text S7 in Supporting Information S1). The stoichiometric analysis indicated that, on average, for every mole of DIC produced in the DZ, 77% originates from translocated DOC from SZ and 23% from deeper carbon sources.

The sorption reaction ($Sorp_{SZ}$) was necessary to capture peak DOC at snowmelt. Without $Sorp_{SZ}$, $C_{STREAM,DOC}$ increased to near peak concentration immediately at the onset of snowmelt in May, and then quickly dropped to

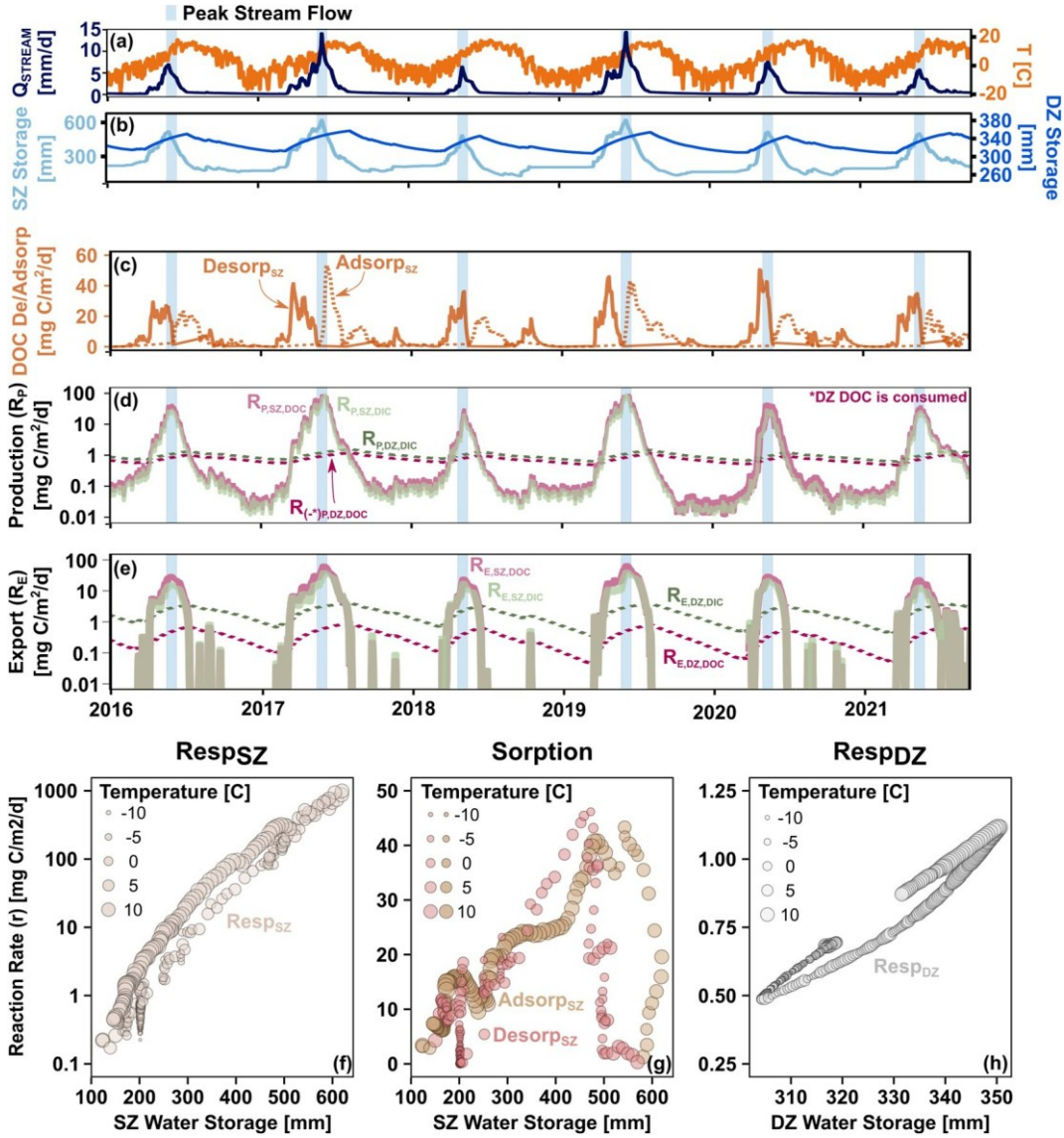

Figure 6. Time series of (a) discharge and air temperature, and modeled (b) water storage, (c) sorption rates (adsorption and desorption), and DOC and DIC (d) production (R_P) and (e) export rates (R_E) in the SZ (solid line) and DZ (dashed line). Daily reaction rates (r) for WY19 representing mg of organic carbon consumed or released to produce DOC and DIC via (f) shallow zone respiration ($Resp_{SZ}$), (g) Sorption ($Adsorp_{SZ}$ and $Desorp_{SZ}$), and (h) deep zone respiration ($Resp_{DZ}$) as a function of storage and temperature. For total mg of DOC or DIC produced (f–h), multiply reaction rate (r) by the stoichiometric coefficients for each reaction (Table 1). Respiration rates peak at maximum water storage in both SZ and DZ; higher temperatures are associated with higher rates but to a much lesser degree compared to water storage. $Desorp_{SZ}$ increased with both SZ storage and temperature. $Adsorp_{SZ}$ rates peaked just below peak water storage and at lower storage high $Adsorp_{SZ}$ rates only occur at higher temperatures.

create a trough of $C_{STREAM,DOC}$ during peak discharge, and only increased to peak $C_{STREAM,DOC}$ at the tail-end of snowmelt as stream flow receded (solid gray line in Figure 5c). Only when $Sorp_{SZ}$ was included as a kinetic rate form could the model capture the timing of peak $C_{STREAM,DOC}$ and the steady increase of $C_{STREAM,DOC}$ with increasing streamflow.

4.4. Hydrology Drives Daily Carbon Production and Export Dynamics (Intra-Year)

The reaction rates showed a seasonal pattern that echoed discharge (Figure 6). $Sorp_{SZ}$ has two annual peaks (Figure 6c). The first one is the desorption of DOC from soils ($Desorp_{SZ}$) to pore water at the start of snowmelt,

and the second peak represents the adsorption of DOC from water back to soils ($Adsorp_{SZ}$) right after peak DOC production at receding streamflow but highest temperatures. Adsorption rates were highest in wet years when $Resp_{SZ}$ rates were high (Figure 6d). In dry years, R_P from $Adsorp_{SZ}$, $Resp_{SZ}$ and $Desorp_{SZ}$ were similar in magnitude but lower compared to wet years. $Resp_{SZ}$ rates, and thus production of DOC and DIC, peaked in early summer when peak snowmelt maximized water storage and rapid flow in the SZ. In other words, at the start of snowmelt, desorption of DOC from previous year contributed to the early rise of DOC, followed by major production of DOC in the same year that sustained the rest of the DOC peak during snowmelt. Some of the produced DOC also sorbed on soils, contributing to the early DOC release in the next year.

Further analysis showed substantial reaction rates only occurred during periods of high soil moisture, while low soil moisture reduced $Resp_{SZ}$ rates, regardless of temperature (Figure 6f). Additionally, production of dissolved carbon from $Resp_{SZ}$ in wet years was almost three times that of those in dry years, further emphasizing water content as a key driver of $Resp_{SZ}$. DZ respiration rates were about one and three orders of magnitude lower than respiration rates in SZ. These DZ respiration rates were stable from year to year, and similarly increased during snowmelt but by a much lesser degree.

Export unsurprisingly followed the trend of discharge. In the SZ, export peaked at peak snowmelt and in wettest years (two times more than in dry years) with fluxes of DOC always exceeding that of DIC (Figure 6e). In the DZ, dissolved carbon export was consistent across the years, and similarly peaked during high flow time. The DOC export rates in DZ however were an order of magnitude lower (Figure 6e) than DIC export rates in the DZ due to concentration differences.

4.5. Hydrology Drives Inter-Year Variations in Production and Export

Annual carbon production rates (R_P) correlate positively with total annual discharge, Q, and shallow zone discharge, Q_{SZ} (Figure 7a) and peaked in wettest years (WY 2017 & WY 2019). While annual production of DOC was typically higher than that of DIC the difference diminished in dry years. Additionally, the annual production of DIC from the SZ was typically higher than that in the DZ, reaching as high as an order of magnitude higher in SZ in wet years (WY17 & 19) (Table S2 in Supporting Information S1). In lower flow years (WY16, 18, 20, & 21), DZ production accounted for an average of 25 ± 13.8% of the total DIC production. Annual production of DOC and DIC from $Resp_{SZ}$ correlated negatively with T_{MAX} and mirrored the relationship of Q with $Resp_{SZ}$. Trends with annual average (T_{AVE}) and annual minimum temperature (T_{MIN}) were also examined (Figure S8 in Supporting Information S1), but clear trends with production were only evident for T_{MAX}.

The annual $Desorp_{SZ}$ rates did not vary as much as respiration rates did between years, or with Q and temperature (Figures 7a and 7b, Table S4 in Supporting Information S1). During wet years, DOC was primarily derived from $Resp_{SZ,DOC}$; however, in drier years, especially when Q was less than ~375 mm/yr, $Desorp_{SZ}$ (of DOC from previous years) became higher and the dominant contributor of DOC in the SZ. In the DZ, respiration consumed DOC to produce DIC, and had similar rates across years (Multi-year mean and standard deviation of total annual $R_{P,DZ,DIC} = 0.36 \pm 0.02$ g C/m^2/yr).

The multi-year mean and standard deviation of total annual export (R_E) of DOC and DIC was 1.75 ± 0.97 and 1.81 ± 0.66 g C/m^2/yr, respectively. However, during the two high-flow years, the total average export increased to 2.97 ± 0.07 g C/m^2/yr for DOC and 2.64 ± 0.16 g C/m^2/yr for DIC, and the SZ was the dominant source. On average, the SZ contributed 73.5 ± 8.7% of total annual stream flow and accounted for 91.3 ± 3.8% and 57.2 ± 12.7% of the total annual export flux of DOC and DIC, respectively. In contrast, the DZ contributed an average of 42.7 ± 12.8% of the total annual DIC export flux, while only contributing 8.7 ± 3.8% of annual DOC export flux. This disparity arose because the DZ generally has much higher concentrations of DIC and contributed to streamflow throughout the year, despite the majority of DIC being produced in the SZ.

Discharge exhibited a strong positive correlation with modeled annual fluxes of DOC and DIC, accounting for 99% of the variation. The measured annual flux of DOC also exhibited a similar positive relationship with discharge explaining 95% of the observed variation in average DOC years. When including all years, discharge explained 76% of the variation (Figure S9 in Supporting Information S1), with the largest outliers being DOC fluxes in the high DOC years of WY17 and WY18. The measured annual flux of DIC correlated positively with discharge across all years and discharge explained 95% of the observed variation.

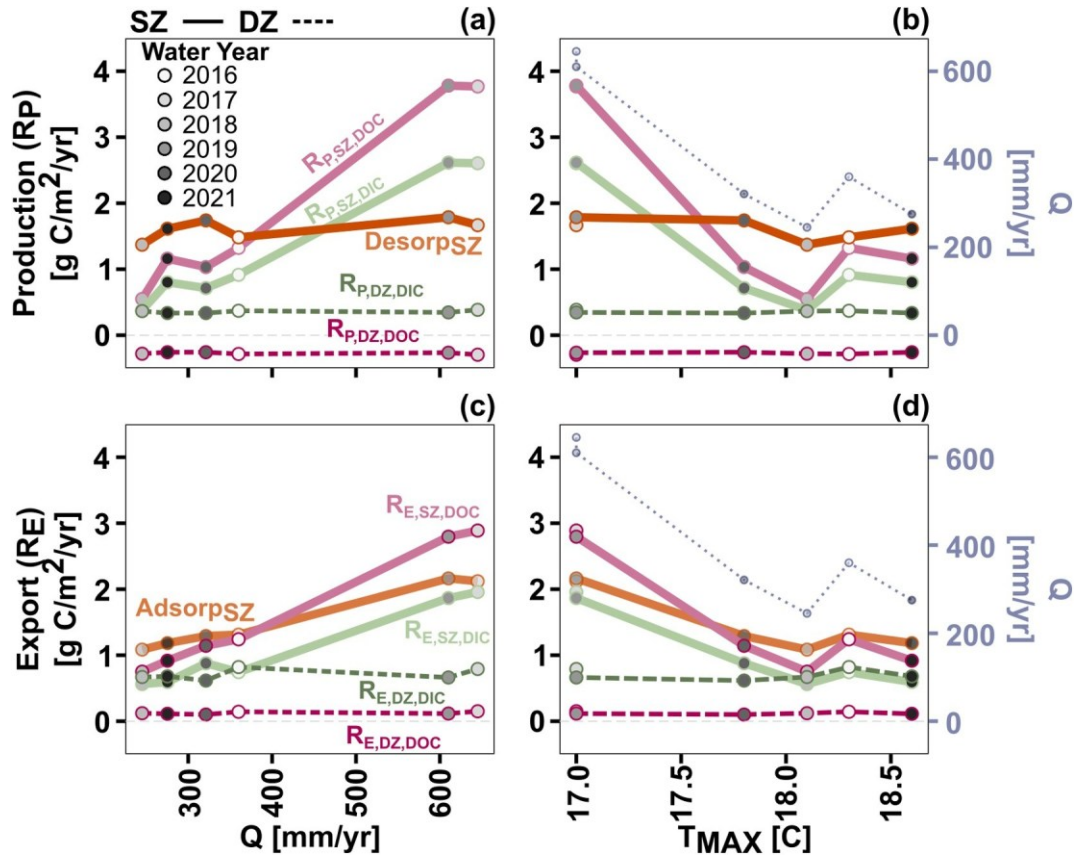

Figure 7. Annual production and export plotted against total annual discharge (Q) and annual maximum temperature (T_{MAX}). At the annual scale, (a) $R_{P,SZ}$ increased with Q, whereas $Desorp_{SZ}$ and $R_{P,DZ}$ were mostly consistent across Q. (b) $R_{P,SZ}$ decreased with T_{MAX}, but $Desorp_{SZ}$ and $R_{P,DZ}$ were consistent across T_{MAX}. The trend of $Resp_{SZ}$ reflected that of Q and T_{MAX} which suggests Q and T_{MAX} correlation. (c) $R_{E,SZ}$ for DOC and DIC increased with large Q, however $R_{E,DZ}$ is consistent with Q. (d) $R_{E,SZ}$ and Q followed the same decreasing trend with T_{MAX}.

4.6. Numerical Experiments of Future Climate Scenarios

Numerical experiments were conducted to understand and project how stream chemistry responds to future climate. The five cases tested include (as detailed in Table 2) (1) sustained dry conditions with highest T_{MAX} (WY21) (Dry-HighT_{MAX}), (2) sustained dry conditions with highest T_{AVE} (WY18) (Dry-HighT_{AVE}), (3) sustained wet conditions with low temperature (WY19) (Wet-LowT), (4) alternating a wet (WY 19) and dry year using the dry year with highest maximum annual temperature (WY21) (Wet-LowT/Dry-HighT_{MAX}), and (5) alternating a wet (WY19) and dry year using the dry water year with highest average annual temperature (WY18) (Wet-LowT/Dry-HighT_{MAX}) over 2021–31. These two dry years were chosen as they have similar total annual discharge but different peak streamflow timing. Each scenario shows a different behavior and can vary for DOC and DIC.

The scenarios revealed contrasting impacts of sustained wet and dry conditions on DOC and DIC concentrations. Sustained wet conditions elevated concentrations of DOC and DIC (Figures 8a and 8b), and enhanced DOC adsorption such that more DOC was sorbed/stored on soil (Figure 8c). On the other hand, the driest case (WY18: Dry-HighT_{AVE}) led to a rapid drop in sorbed DOC (Figure 8c) and reduced aqueous concentrations (Figures 8a and 8b), suggesting low DOC production such that less DOC is stored in the subsurface.

Despite a relatively small difference in Q (~10%) between the two dry cases, average concentrations showed a decreasing trend for Dry-HighT_{AVE} (WY18) and an increasing trend for Dry-HighT_{MAX} (WY21) (Figures 8a and 8b). These concentration changes can be primarily attributed to differences in production rates within the SZ. Notably, peak production of both DOC and DIC aligns with peak discharge for both cases. However, in Dry-HighT_{MAX} peak discharge and production occurred later in the year during higher temperatures (Figures 8d

10.1029/2023WR036077

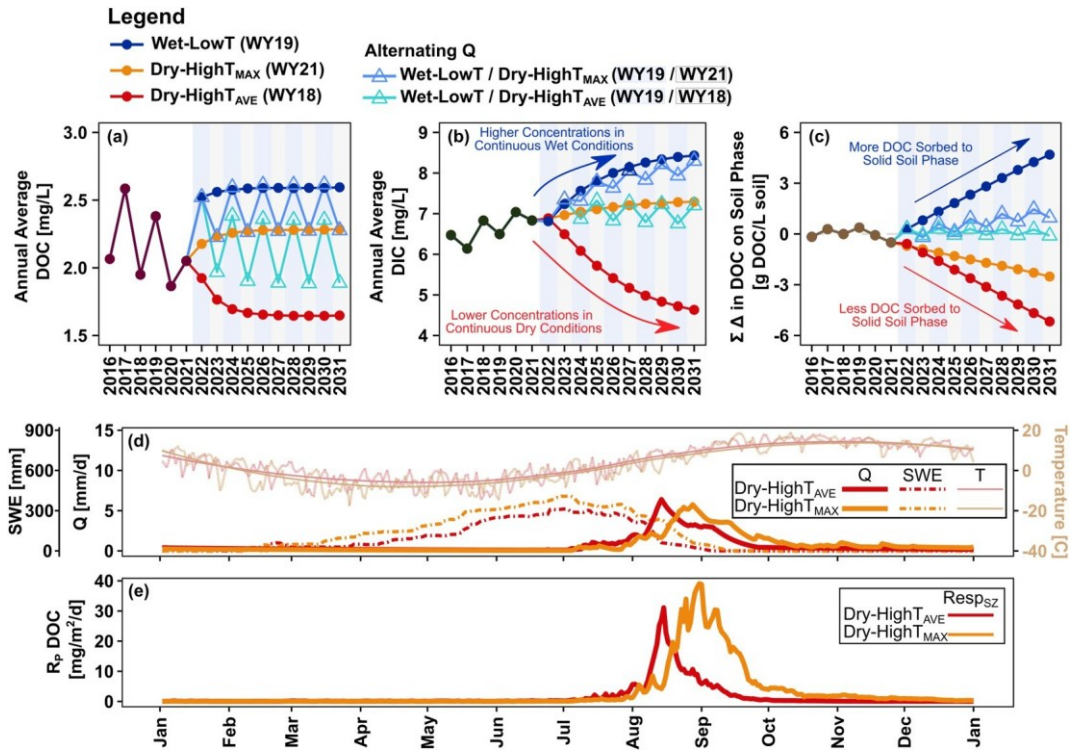

Figure 8. Numerical experiments for five cases (details in Table 2): (1) sustained dry conditions with highest TMAX (WY21) (Dry-HighTMAX), (2) sustained dry conditions with highest T_{AVE} (WY18) (Dry-HighT_{AVE}), (3) sustained wet conditions with low temperature (WY19) (Wet-LowT), (4) alternating a wet (WY 19) and dry year using the dry year with highest maximum annual temperature (WY21) (Wet-LowT/Dry-HighT$_{MAX}$), and (5) alternating a wet (WY19) and dry year using the dry water year with highest average annual temperature (WY18) (Wet-LowT/Dry-HighT$_{MAX}$). (a) Average annual DOC concentrations increase for all cases except for the alternating and continuous dry case with Dry-HighT$_{AVE}$ (WY18). In the alternating cases high DOC concentrations occur in wet years (light blue background). (b) DIC concentrations generally increase except for the Dry-HighT$_{AVE}$ (WY18) case, and in alternating cases DIC concentrations are highest in low flow years (gray background). (c) Sustained dry conditions cause a net loss of DOC from the solid phase and sustained wet conditions cause a net increase. Alternating conditions show gains in wet years and losses in dry years, with a long-term trend that hovers around zero. (d) Peak discharge occurs earlier for Dry-HighT$_{AVE}$ (WY18) than Dry-HighT$_{MAX}$ (WY21), however, Q is similar for each case. (e) Dry-HighT$_{AVE}$ (WY18) shows earlier peak production (R_P) and less overall production than Dry-HighT$_{MAX}$ (WY21) in the SZ.

and 8e). The higher soil moisture of Dry- HighT$_{MAX}$, in the warmer summer months enhanced annual $R_{P,DOC}$ and $R_{P,DIC}$ by 52.7% and 34.6%, respectively (Table S2 in Supporting Information S1), compared to Dry-HighT$_{AVE}$ where the cooler temperature earlier in the year resulted in lower reaction rates. These findings underscore the complex interplay between discharge patterns temperature, and biogeochemical processes in shaping the carbon dynamics in Coal Creek.

5. Discussion

This study aims to illuminate the often-overlooked subsurface processes that drive dissolved carbon production and export. We aimed to address the questions: *1) What are the predominant drivers of dissolved carbon production in rapidly changing, snow-dominated montane catchments? 2) How much dissolved carbon is produced and exported via the shallow and deep subsurface at daily, seasonal, and annual scales?* The reactive transport model links the subsurface hydrological and biogeochemical processes to stream carbon dynamics and quantifies the concentrations and fluxes of dissolved carbon. It offers mechanistic, in-depth view of biogeochemical reactions and flow paths that regulate DOC and DIC production and export and their stream dynamics (Figure 9).

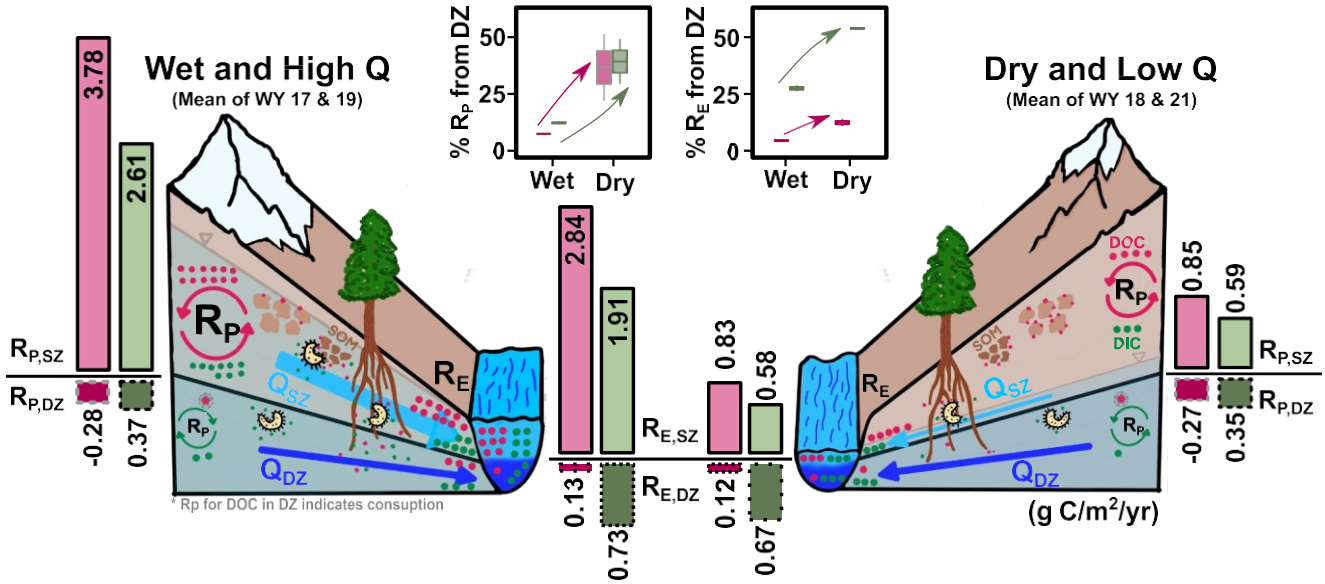

Figure 9. Conceptual figure illustrating dissolved carbon production (R_P; g C/m^2/yr) and export (R_E; g C/m^2/yr) in wet (WY 17 & 19) and dry (WY 18 & 21) years. In wet, high Q conditions (left), higher shallow flow and production rates promote more carbon export compared to the drier conditions. Under dry, low Q conditions (right) with a deep water table, production rates in the shallow zone (SZ) and deep zone (DZ) are low, leading to more DOC sorbed on soils and reduced export. Although R_P and R_E are lower in the DZ than the SZ in both conditions, there is a notable increase in the contribution of DZ R_P and R_E in drier conditions, indicating the increasing importance of DZ processes as mountain systems become warmer and drier.

5.1. Model Choices and Limitations

Here we choose to use a simple but not simplistic approach to model reactive transport processes. The slim reaction network includes three major lumped reactions that are essential to capture stream carbon dynamics. The model is spatially implicit and represents the average catchment-scale behavior without explicitly accounting for variations in landscape positions. Such simplifications are necessary due to the lack of spatial data to support complex model parameterization and to avoid unnecessary equifinality (Li et al., 2017). The iterative HBV and BioRT calibration balanced constraints from stream flow and chemistry data with a priori site knowledge. The model does not represent instream sources of DOC or DIC such as algae or respiration that can become important in warm, stagnated stream water in late summer, as discussed later. Rather, BioRT-HBV quantifies the soil respiration rates that contribute dissolved carbon to the stream, excluding the soil CO_2 effluxes back to the atmosphere that often represent a large portion of produced CO_2 (Bond-Lamberty et al., 2020; Davidson & Janssens, 2006; Jian et al., 2021). The rates here, therefore, likely underestimate total soil respiration rates. By considering shallow soil and deeper groundwater zones, it does, however, capture first-order variations in abundance of dissolved carbon, hydrological flow paths, and biogeochemical reactions at different depths. It satisfactorily reproduces stream carbon dynamics with a slim number of reactions, suggesting the influential role of these reactions in regulating stream chemistry.

5.2. Greater Fractions of Deep Groundwater Under Drier Conditions

The hydrology in Coal Creek is primarily driven by snowmelt, typical for high-elevation, snow-dominated mountain catchments in the northern hemisphere (Finger et al., 2015; Harrison et al., 2021). Model results indicated that ~76% of the stream discharge (multi-year average) is from snowmelt, similar to the ~74% average calculated for the Rockies (Pfister et al., 2017). The multi-year average ET and runoff ratios were 468.13 ± 28.1 mm and 0.41 ± 0.08, respectively, about 10%–20% lower than the estimated numbers in 2016 at this site (Zhi et al., 2019). These numbers are generally within the range of 490.2 ± 49.4 mm and 0.40 to 0.60 in high-elevation catchments in the Upper Colorado River Basin (Lukas & Payton, 2020; Ryken et al., 2022).

Model results showed an average groundwater fraction ($f(Q_{DZ})$) of 26.3 ± 8.9%, close to previously estimated 20% in Coal Creek (Zhi et al., 2019) and falls on the lower end of the 12%–92% range documented in the Upper Colorado River Basin (Rumsey et al., 2015). Similar to the deeper flow fraction of 35 ± 7% in the adjacent, similar

relief catchment, Copper Creek (Carroll et al., 2018, 2019). In Copper Creek, deeper flow fractions escalate under drier conditions at the expense of decreased lateral flow through the SZ (Carroll et al., 2019). In Coal Creek, although DZ storage and flow rates remain similar across years, deeper water fractions increase due to lower flow in SZ and overall lower total discharge in drier years (K. Johnson et al., 2023). Steep high-elevation catchments with higher SZ water fractions have been observed to exhibit more pronounced response to warming (Hare et al., 2021). With a high fraction of shallow flow, Coal Creek could be more responsive to climate than catchments with greater deeper groundwater flow contributions (Blaurock et al., 2021; Carroll et al., 2019; Hare et al., 2021).

5.3. Substantial Deep Respiration Shapes Concentration-Discharge Relationships

Existing literature has focused more on shallow soil respiration compared to deeper respiration (Davidson & Janssens, 2006; Keller, 2019; Marx et al., 2017; Tank et al., 2018). Deep respiration can occur via roots, the oxidation of DOC transported to the DZ from the SZ, and also by the oxidation of deep organic carbon (Tune et al., 2020). Although the estimated deep respiration rates are an order of magnitude lower than in shallow soil, it occurs across the year, contributing a substantial amount, on average (27 ± 14%), of overall DIC produced in the catchment. Strikingly, the proportion of DIC from deep respiration rises to >50% in the driest year, indicating the increasing importance of deep processes as conditions become drier. This echoes recent observations that respiration rates in bedrock can occur at similar rates as those in shallow soils (Hasenmueller et al., 2017; Tune et al., 2020, 2023), challenging the traditional perception that subsurface carbon dynamics are regulated top down and dominated by the shallow zone. Such insights highlight the integral role of deep processes in carbon cycling and acknowledging both shallow and deep processes offers a more comprehensive understanding of terrestrial-aquatic carbon dynamics.

Coal Creek's stream carbon exhibits the commonly observed flushing pattern (increasing concentration discharge) for DOC (Boyer et al., 2000; Raymond & Saiers, 2010; Zarnetske et al., 2018; Zhi et al., 2019) and dilution pattern (decreasing concentration with discharge) for DIC (Marx et al., 2017; Perdrial et al., 2014; Stewart, Zhi, et al., 2022). These patterns have been explained by the shallow and deep hypothesis where shallow and deep flows carry distinct chemical signatures that indicate different processes at different subsurface depths (Musolff et al., 2015; Stewart, Shanley, et al., 2022; Zhi & Li, 2020).

This work suggests that deep respiration processes primarily shape such distinct patterns of dissolved carbon. DOC has been commonly observed to show flushing CQ pattern with concentrations in increasing with stream discharge (Zarnetske et al., 2018). Without deep respiration consuming DOC, DOC concentrations in the deep zone would eventually reach the same level as the SZ, resulting in a chemostatic CQ relationship (Figure 5b) with similar stream DOC concentrations under high and low flow regimes. On the other hand, deep respiration adds DIC in the deep zone, leading to commonly observed increasing DIC concentrations with depth and the near-universal dilution CQ pattern (Stewart, Shanley, et al., 2022). This rise in DIC concentration with depth is often attributed to CO_2 loss to the atmosphere in top soil (Keller, 2019) and rapid export during high flow events (Wen et al., 2022). It has also been attributed to carbonate weathering that can elevate DIC concentrations in the deep subsurface (Marx et al., 2017; Xianwei et al., 2021). Coal Creek, however, has limited sources of carbonates (Gaskill et al., 1967, 1987) and shows much lower stream DIC concentrations compared to an adjacent catchment with known DIC contributions from carbonates (Figure S16 in Supporting Information S1). Results here therefore suggest that the additional deep respiration elevates DIC concentrations in the DZ compared to the SZ (Stewart, Shanley, et al., 2022), generating the universally observed dilution CQ patterns for DIC.

5.4. Hydrology (Not Temperature) as the Predominant Driver of Dissolved Carbon Production

Daily production rates in Coal Creek, which varied little with temperature but increased substantially with soil moisture, reveal the critical role of hydrologic conditions (Figure 6). This pattern extended to annual scales where production rates exhibit zero or negative correlations with temperature, but significant positive correlations with discharge. And, similar to other snow dominated catchments, total discharge and T_{MAX} are negatively correlated (Winterdahl et al., 2014), and higher production only occurs during wetter times, even under cooler conditions. In Coal Creek, this hydrology limitation leads to the concurrent peak of production and export during peak snowmelt and might be distinctive to arid or semi-arid climates. This contrasts more humid sub-tropical, temperate, and boreal catchments where simultaneous peaks arise due to the co-occurrence of wet and hot seasons and production

rates are often strongly dependent on temperature (Dawson et al., 2008; Perdrial et al., 2014; Wen et al., 2020, 2024; Winterdahl et al., 2016). This supports the idea that soil moisture influences production more in seasonally defined catchments with large fluctuations in soil moisture (Li et al., 2017). For example, in the temperate-humid catchment, Shale Hills, soil saturation varies within a relatively narrow range (0.46–0.56, (Wen et al., 2020)), compared to 0.27–0.62 in Coal Creek. Although having similar maximum soil saturation values, Coal Creek exhibits lower saturation values during dry times, closer to other arid sites that see minimum saturation values as low as 0.15 (Korres et al., 2015). In other words, it is possible that in more arid, water-limited places, temperature dependence only arises under wet conditions, thus reaction rates depend more on water content and hydrology than temperature.

Temperature influence arising only in times of adequate soil moisture is exemplified by comparing the two dry years (WY 18; dry year with high T_{AVE}; WY21, dry year with high T_{MAX}) with similar total discharge. WY18 exhibited earlier snowmelt and returned to baseflow by the end of June when lower temperatures can still persist, in contrast WY 21 experienced peak flow at the end of May and only returned to baseflow after July, when summer temperatures were higher. Indicating that higher temperatures need to coincide with times of adequate soil moisture for temperature to drive greater soil respiration rates (Correia et al., 2012; Stielstra et al., 2015). The interplay of temperature with soil moisture is particularly pronounced in the divergent climate scenario results. Average stream concentrations of DOC and DIC increase under sustained conditions of Dry-HighT_{MAX} but decrease under Dry-HighT_{AVE}, suggesting if climate change shifts snowmelt earlier carbon production and export may decrease unless accompanied by higher temperatures during this earlier snowmelt period.

The western US is projected to experience increased precipitation variability, although the trend of precipitation in the Upper Colorado River basin has remained relatively leveled or slightly increased (~1920–2020) (Milly & Dunne, 2020; M. Xiao et al., 2018). If this shift in precipitation favors significant rainfall events during the warm summer months (e.g., larger summer monsoons common in this region) that exceed the ET demand (Carroll et al., 2020; Sprenger et al., 2022), it could lead to favorable soil moisture conditions for enhanced soil respiration during the summer (Stielstra et al., 2015) and potentially elevated stream carbon concentrations. The soil moisture dependence in BioRT also emphasizes hydrologic importance by representing-stream connectivity. High soil moisture and a high water table suggest a more hydrologically connected catchment (Jencso et al., 2009; Weyman, 1973) which can enable contributions from more hydrologically distant hotspots to streams. Such hot spots of DOC generation could include wetlands (Bhattacharya & Osburn, 2020; Elder et al., 2000; Hinton et al., 1998) which exist in the upper stream reaches and on south-facing hillslopes in Coal Creek. The peak reaction rates at peak discharge potentially suggest the contribution of these hotspots under wet conditions in more hydrologically connected catchment (Inamdar & Mitchell, 2006; Pesántez et al., 2023).

Sorption dynamics are significantly influenced by hydrology and play a crucial role in regulating the timing of peak DOC concentrations, mirroring distinct phases of DOC dynamics observed in a sub-arctic snow-melt dominated catchment (Tang et al., 2018). Initially, snowmelt triggers desorption, releasing DOC previously produced and adsorbed on soils. As snowmelt continues and the water table rises desorption remains the primary source for DOC until its stores on soils are depleted. At this point, production via soil respiration peaks and predominates the DOC pool (Figure 6). After peak production, the third phase commences, during which the newly produced DOC increases porewater concentrations to drive DOC adsorption onto soils. In other words, soils act as a storage reservoir where DOC is flushed out during snowmelt events subsequent to times of DOC production and adsorption (Wen et al., 2020). Most DOC adsorption occurred during wet years, which indicates wet years enhance DOC storage which is then released via desorption in dry years.

5.5. Hydrology-Driven Export of Dissolved Carbon

The export of DOC and DIC peak during snowmelt and in wet years. DOC and DIC export can reach as high as 3.04 and 2.75 g C/m^2/yr, respectfully, in wet years, almost on par with those from tropical rivers (DOC = 3.16 g C/m^2/yr; DIC = 3.33 g C/m^2/yr (Huang et al., 2012)), while DOC and DIC export in dry years can be three times lower. Although humid tropical climates are typically associated with highest carbon yields (Brantley et al., 2017), these high values at Coal Creek corroborate that low-order streams in small mountain catchments are hot spots for export of dissolved carbon and CO_2 emission (Bao et al., 2015; Horgby et al., 2019; Raymond et al., 2013). Indicating the high potential for altered carbon cycling under warming conditions in mountain systems. Mean annual export correlated negatively with T_{MAX} (Figure 7d), suggesting higher

temperature reduces discharge and export capacity in warmer years. This entangled temperature and discharge influence on DOC export is consistent with other snow-dominated and high-elevation catchments that exhibit a highly seasonal flow regime (Meingast et al., 2020; Winterdahl et al., 2014). In other words, temperature can elevate ET and thus reduce water content emphasizing the dominant role discharge plays in controlling export rates.

It is noteworthy that over 90% of annual lateral export of DOC occurs through shallow flow paths, underscoring the importance of wetter conditions in driving DOC fluxes via shallow soils (Zhi & Li, 2020; Zhi et al., 2019). DOC only peaks at peak discharge when the catchment is most hydrologically connected, potentially suggesting contributions from high DOC stores in the shallow soils from hydrologically distant sources (Abbott et al., 2016; Adler et al., 2021), such as wetlands discussed in the previous section. This is also consistent with the necessity of using slower, kinetically controlled sorption/desorption with dependence on soil moisture to reproduce the timing of DOC peaks. In fact, our initial attempt of using a fast, equilibrium-controlled sorption mechanism consistently led to earlier peak DOC and a significant concentration dip during peak snowmelt. This implies the gradual mobilization of DOC from afar as the water table rises, expands, and connects to distant uphill slopes.

Deep flow paths can account for >50% of the annual DIC export in Coal Creek. In other catchments, up to 60% of annual DIC flux have been observed to occur via shallow flow paths, indicating equal or predominant DIC export fluxes via deeper flow paths (Tune et al., 2020). Greater contributions from the deeper zone have been associated with lower permeability contrasts between the SZ and DZ that enhance higher vertical connectivity (Wen et al., 2022; D. Xiao et al., 2021). Additionally, at sites with carbonate lithology, carbonate weathering can further increase DIC production and export via deeper flow paths (Marx et al., 2017; Xianwei et al., 2021). In Coal Creek ~75% of streamflow comes from Q_{SZ} and ~25% from Q_{DZ}, indicating a higher SZ-DZ permeability contrast. And with limited carbonates, the large difference in deep DOC and DIC fluxes arises from their notable disparity in concentration within the DZ with $C_{DZ,DOC}$ at 1.23 ± 0.14 mg/L and $C_{DZ,DIC}$ at 7.52 ± 2.8 mg/L. These findings underscore the importance of considering both shallow and deep flow paths to fully comprehend the dynamics of dissolved carbon export. Especially under warmer and drier conditions when deep groundwater flow paths become more important.

5.6. In-Stream Respiration and CO_2 Evasion

Stream data consistently showed a recurring "bump" in DIC concentrations every year during the summer months following snowmelt, which the model failed to reproduce. Similar increases in stream DIC concentrations post event-flow have been observed in other catchments, often persisting from hours (M. S. Johnson et al., 2007) to weeks (Demars, 2019; Perdrial et al., 2014). Various explanations for this DIC increase have been proposed, including changes in CO_2 evasion rates and additional CO_2 input from delayed flow paths (M. S. Johnson et al., 2007). In Coal Creek, this DIC bump coincides with the warm summer growing season during low flow subsequent to the influx of fresh DOC from snowmelt, all of which maximize stream and riparian respiration (Doctor et al., 2008). Additionally, reduced dissolved oxygen (DO) concentration has been observed at this time (Figure S14 in Supporting Information S1), similar patterns of increased DIC and decreased DO due to CO_2 production have been observed in other forested streams (Allan, 1995; Perdrial et al., 2014). Thus, the post-snowmelt "bump" in DIC is likely attributed to instream respiration processes. Currently, our model does not consider these instream processes that generate CO_2 and increase DIC concentrations, which may explain the discrepancy between the observed data and modeled results.

In Coal Creek, this post snow-melt DIC bump accounts for an average of 4.8 ± 3% of DIC input to streams annually, much smaller than estimates (~19%) in other headwater streams (Tobias & Böhlke, 2011; Wang et al., 2021). This may be due to the short residence time of DOC in high relief streams and the relatively low temperatures in high elevation mountains that limits the extent of instream respiration (Liu et al., 2022). Broadly, in small mountain streams, DIC largely originates from terrestrial sources (Hotchkiss et al., 2015; Vannote et al., 1980).

Instream production of DIC exhibits negative trends with annual temperature metrics but a positive trend with Q (Figures S10 and S11 in Supporting Information S1). Although the trends were not statistically significant for the 6 years analyzed, they suggest that instream processes become a greater contributor to stream DIC levels during low flow conditions. This is because, even though total instream DIC production may be lower, the terrestrial flux of DIC to streams is also reduced. Elevated DIC concentrations can enhance stream CO_2 evasion, especially in the

growing season when in-stream CO_2 production from respiration elevates (Doctor et al., 2008). However, the magnitude of this effect is highly uncertain, as CO_2 evasion depends not only on DIC concentration but also on factors such as pH, flow rates, turbulent flow dynamics, and other catchment characteristics.

6. Conclusion

Understanding the intertwined hydrological and biogeochemical processes in the shallow and deep subsurface and how they drive the terrestrial production and lateral export of dissolved carbon has been a long-standing challenge. Here we used a catchment-scale reactive transport model to gain a mechanistic understanding of the interactive hydrological and biogeochemical processes that regulate dissolved carbon production and export in a snow-dominated high elevation headwater catchment in the Rocky Mountains. The results reveal that in this water-limited catchment, hydrology predominantly drives both production and export of dissolved carbon, contrasting the distinct roles of hydrology and temperature in controlling export and production, respectively, in temperate, wetter climates (Wen et al., 2020). Shallow soils dominate the production and export of carbon, but the deep zone produces and exports a substantial fraction of dissolved carbon, which increased in drier years. DOC production rates peaked during snow melt and wet years, with sorption acting as the primary storage mechanism in between years. DOC was primarily produced in the shallow subsurface and consumed in the deeper subsurface, with more export from the shallow zone compared to the deep zone. This deep respiration is responsible for the commonly-observed increasing DOC concentrations (flushing) (Kincaid et al., 2024) and decreasing DIC concentrations (dilution) with increasing discharge (Stewart, Zhi, et al., 2022). DIC production similarly peaked during snow melt and wet years and is exported in comparable quantities in the shallow subsurface than in the deep subsurface. Numerical experiments suggest that under warmer and drier climates that promote earlier snowmelt, the production and export of dissolved carbon will drop mainly in the shallow soils but not as much in the deeper zone. This suggests an amplified influence of deeper flow and deeper respiration in the future warmer, drier climate.

Data Availability Statement

Data: Streamflow and stream carbon data are available in Dong et al. (2024) via the ESS-DIVE online data repository. Model input and output files use for this study are available at Kerins et al. (2023). *Software*: Source code and example files for BioRT-HBV are available at Sadayappan et al. (2024b).

Acknowledgments

This work is supported by the Department of Energy Environmental System Science (DE-SC0020146) and National Science Foundation Critical Zone Coordination Network (EAR-2012669 and EAR-2012123) and Frontier Research in Earth Sciences (EAR-2121621). This material is partially based upon work supported through the Lawrence Berkeley National Laboratory's Watershed Function Focus Area. The U.S. Department of Energy (DOE), Office of Science, Office of Biological and Environmental Research funded the work under contract DE-AC02-05CH11232 (Lawrence Berkely National Laboratory; operated by the University of California). We thank Wendy Brown for her tireless work in maintaining the Coal-11 ISCO water sampler and for stream water sample collection over the years for which data was used to support the findings presented herein. Additionally, we thank Dr. Mark Johnson and two anonymous reviewers for their thorough and helpful suggestions, as well as Dr. Simone Fatichi for additional suggestions and handling the manuscript.

References

Abbott, B. W., Baranov, V., Mendoza-Lera, C., Nikolakopoulou, M., Harjung, A., Kolbe, T., et al. (2016). Using multi-tracer inference to move beyond single-catchment ecohydrology. *Earth-Science Reviews*, *160*, 19–42. https://doi.org/10.1016/j.earscirev.2016.06.014

Adler, T., Underwood, K. L., Rizzo, D. M., Harpold, A., Sterle, G., Li, L., et al. (2021). Drivers of dissolved organic carbon mobilization from forested headwater catchments: A multi scaled approach. *Frontiers in Water*, *3*. https://doi.org/10.3389/frwa.2021.578608

Allan, J. (1995). *Stream ecology: Structure and function of running waters*. Chapman and Hall.

Bales, R. C., Molotch, N. P., Painter, T. H., Dettinger, M. D., Rice, R., & Dozier, J. (2006). Mountain hydrology of the western United States. *Water Resources Research*, *42*(8). https://doi.org/10.1029/2005wr004387

Bao, H., Lee, T. Y., Huang, J. C., Feng, X., Dai, M., & Kao, S. J. (2015). Importance of Oceanian small mountainous rivers (SMRs) in global land-to-ocean output of lignin and modern biospheric carbon. *Scientific Reports*, *5*(1), 16217. https://doi.org/10.1038/srep16217

Barba, J., Cueva, A., Bahn, M., Barron-Gafford, G. A., Bond-Lamberty, B., Hanson, P. J., et al. (2018). Comparing ecosystem and soil respiration: Review and key challenges of tower-based and soil measurements. *Agricultural and Forest Meteorology*, *249*, 434–443. https://doi.org/10.1016/j.agrformet.2017.10.028

Barnes, R. T., Butman, D. E., Wilson, H. F., & Raymond, P. A. (2018). Riverine export of aged carbon driven by flow path depth and residence time. *Environmental Science & Technology*, *52*(3), 1028–1035. https://doi.org/10.1021/acs.est.7b04717

Beck, H. E., van Dijk, A. I. J. M., de Roo, A., Miralles, D. G., McVicar, T. R., Schellekens, J., & Bruijnzeel, L. A. (2016). Global-scale regionalization of hydrologic model parameters. *Water Resources Research*, *52*(5), 3599–3622. https://doi.org/10.1002/2015wr018247

Bergström, S. (1976). In *Development and application of a conceptual runoff model for Scandinavian catchments* (Vol. RHO 7). SMHI.

Bhattacharya, R., & Osburn, C. L. (2020). Spatial patterns in dissolved organic matter composition controlled by watershed characteristics in a coastal river network: The Neuse River Basin, USA. *Water Research*, *169*, 115248. https://doi.org/10.1016/j.watres.2019.115248

Blaurock, K., Beudert, B., Gilfedder, B. S., Fleckenstein, J. H., Peiffer, S., & Hopp, L. (2021). Low hydrological connectivity after summer drought inhibits DOC export in a forested headwater catchment. *Hydrology and Earth System Sciences*, *25*(9), 5133–5151. https://doi.org/10.5194/hess-25-5133-2021

Bond-Lamberty, B., Christianson, D. S., Malhotra, A., Pennington, S. C., Sihi, D., AghaKouchak, A., et al. (2020). COSORE: A community database for continuous soil respiration and other soil-atmosphere greenhouse gas flux data. *Global Change Biology*, *26*(12), 7268–7283. https://doi.org/10.1111/gcb.15353

Botter, M., Li, L., Hartmann, J., Burlando, P., & Fatichi, S. (2020). Depth of solute generation is a dominant control on concentration-discharge relations. *Water Resources Research*, *56*(8). https://doi.org/10.1029/2019wr026695

Boyer, E. W., Hornberger, G. M., Bencala, K. E., & Mcknight, D. M. (1997). Response characteristics of DOC flushing in an alpine catchment. *Hydrological Processes*, *11*(12), 1635–1647. https://doi.org/10.1002/(sici)1099-1085(19971015)11:12<1635::aid-hyp494>3.0.co;2-h

Boyer, E. W., Hornberger, G. M., Bencala, K. E., & McKnight, D. M. (2000). Effects of asynchronous snowmelt on flushing of dissolved organic carbon: A mixing model approach. *Hydrological Processes*, *14*(18), 3291–3308. https://doi.org/10.1002/1099-1085(20001230)14:18<3291::Aid-hyp202>3.0.Co;2-2

Brantley, S. L., McDowell, W. H., Dietrich, W. E., White, T. S., Kumar, P., Anderson, S. P., et al. (2017). Designing a network of critical zone observatories to explore the living skin of the terrestrial Earth. *Earth Surface Dynamics*, *5*(4), 841–860. https://doi.org/10.5194/esurf-5-841-2017

Brookfield, A. E., Hansen, A. T., Sullivan, P. L., Czuba, J. A., Kirk, M. F., Li, L., et al. (2021). Predicting algal blooms: Are we overlooking groundwater? *Science of the Total Environment*, *769*, 144442. https://doi.org/10.1016/j.scitotenv.2020.144442

Brooks, P. D., Grogan, P., Templer, P. H., Groffman, P., Öquist, M. G., & Schimel, J. (2011). Carbon and nitrogen cycling in snow-covered environments. *Geography Compass*, *5*(9), 682–699. https://doi.org/10.1111/j.1749-8198.2011.00420.x

Burns, M. A., Barnard, H. R., Gabor, R. S., McKnight, D. M., & Brooks, P. D. (2016). Dissolved organic matter transport reflects hillslope to stream connectivity during snowmelt in a montane catchment. *Water Resources Research*, *52*(6), 4905–4923. https://doi.org/10.1002/2015wr017878

Carroll, R. W. H., Bearup, L. A., Brown, W., Dong, W., Bill, M., & Willlams, K. H. (2018). Factors controlling seasonal groundwater and solute flux from snow-dominated basins. *Hydrological Processes*, *32*(14), 2187–2202. https://doi.org/10.1002/hyp.13151

Carroll, R. W. H., Deems, J., Sprenger, M., Maxwell, R., Brown, W., Newman, A., et al. (2022). Modeling snow dynamics and stable water isotopes across mountain landscapes. *Geophysical Research Letters*, *49*(20). https://doi.org/10.1029/2022gl098780

Carroll, R. W. H., Deems, J. S., Niswonger, R., Schumer, R., & Williams, K. H. (2019). The importance of interflow to groundwater recharge in a snowmelt-dominated headwater basin. *Geophysical Research Letters*, *46*(11), 5899–5908. https://doi.org/10.1029/2019gl082447

Carroll, R. W. H., Gochis, D., & Williams, K. H. (2020). Efficiency of the summer monsoon in generating streamflow within a snow-dominated headwater basin of the Colorado River. *Geophysical Research Letters*, *47*(23). https://doi.org/10.1029/2020gl090856

Clark, M. P., Kavetski, D., & Fenicia, F. (2011). Pursuing the method of multiple working hypotheses for hydrological modeling. *Water Resources Research*, *47*(9). https://doi.org/10.1029/2010wr009827

Clow, D. W., & Mast, M. A. (2010). Mechanisms for chemostatic behavior in catchments: Implications for CO_2 consumption by mineral weathering. *Chemical Geology*, *269*(1–2), 40–51. https://doi.org/10.1016/j.chemgeo.2009.09.014

Conant, R. T., Ryan, M. G., Ågren, G. I., Birge, H. E., Davidson, E. A., Eliasson, P. E., et al. (2011). Temperature and soil organic matter decomposition rates—Synthesis of current knowledge and a way forward. *Global Change Biology*, *17*(11), 3392–3404. https://doi.org/10.1111/j.1365-2486.2011.02496.x

Correia, A. C., Minunno, F., Caldeira, M. C., Banza, J., Mateus, J., Carneiro, M., et al. (2012). Soil water availability strongly modulates soil CO_2 efflux in different Mediterranean ecosystems: Model calibration using the Bayesian approach. *Agriculture, Ecosystems & Environment*, *161*, 88–100. https://doi.org/10.1016/j.agee.2012.07.025

Crawford, J. T., Hinckley, E.-L. S., Litaor, M. I., Brahney, J., & Neff, J. C. (2019). Evidence for accelerated weathering and sulfate export in high alpine environments. *Environmental Research Letters*, *14*(12), 124092. https://doi.org/10.1088/1748-9326/ab5d9c

Davidson, E. A., & Janssens, I. A. (2006). Temperature sensitivity of soil carbon decomposition and feedbacks to climate change. *Nature*, *440*(7081), 165–173. https://doi.org/10.1038/nature04514

Dawson, J. J. C., Soulsby, C., Tetzlaff, D., Hrachowitz, M., Dunn, S. M., & Malcolm, I. A. (2008). Influence of hydrology and seasonality on DOC exports from three contrasting upland catchments. *Biogeochemistry*, *90*(1), 93–113. https://doi.org/10.1007/s10533-008-9234-3

Dean, J. F. (2019). Groundwater dependent ecosystems in arid zones can use ancient subterranean carbon as an energy source in the local food web. *Journal of Geophysical Research: Biogeosciences*, *124*(4), 733–736. https://doi.org/10.1029/2019jg005089

Demars, B. O. L. (2019). Hydrological pulses and burning of dissolved organic carbon by stream respiration. *Limnology & Oceanography*, *64*(1), 406–421. https://doi.org/10.1002/lno.11048

Doctor, D. H., Kendall, C., Sebestyen, S. D., Shanley, J. B., Ohte, N., & Boyer, E. W. (2008). Carbon isotope fractionation of dissolved inorganic carbon (DIC) due to outgassing of carbon dioxide from a headwater stream. *Hydrological Processes*, *22*(14), 2410–2423. https://doi.org/10.1002/hyp.6833

Dong, W., Beutler, C., Brown, W., Newman, A., O'Ryan, D., Versteeg, R., & Williams, K. (2024). Dissolved inorganic carbon and dissolved organic carbon data for the East River Watershed, Colorad (2015-2023) [Dataset]. *Watershed Function SFA*. https://doi.org/10.15485/1660459

Duvert, C., Butman, D. E., Marx, A., Ribolzi, O., & Hutley, L. B. (2018). CO_2 evasion along streams driven by groundwater inputs and geomorphic controls. *Nature Geoscience*, *11*(11), 813–818. https://doi.org/10.1038/s41561-018-0245-y

Elder, J. J., Rybicki, N. B., Carter, V., & Weintraub, V. (2000). Sources and yields of dissolved carbon in northern Wisconsin stream catchments with differing amounts of peatland. *Wetlands*, *20*(1), 113–125. https://doi.org/10.1672/0277-5212(2000)020[0113:SAYODC]2.0.CO;2

Fang, Z., Carroll, R. W. H., Schumer, R., Harman, C., Wilusz, D., & Williams, K. H. (2019). Streamflow partitioning and transit time distribution in snow-dominated basins as a function of climate. *Journal of Hydrology*, *570*, 726–738. https://doi.org/10.1016/j.jhydrol.2019.01.029

Finger, D., Vis, M., Huss, M., & Seibert, J. (2015). The value of multiple data set calibration versus model complexity for improving the performance of hydrological models in mountain catchments. *Water Resources Research*, *51*(4), 1939–1958. https://doi.org/10.1002/2014wr015712

Gaskill, D. L., DeLong, J. E., & Cochran, D. M. (1987). *Geologic map of the Mt. Axtell quadrangle*. United States Geological Survey.

Gaskill, D. L., Godwin, L. H., & Mutschler, F. E. (1967). Geologic map of the oh-be-joyful quadrangle.

Grandi, G., & Bertuzzo, E. (2022). Catchment dissolved organic carbon transport: A modeling approach combining water travel times and reactivity continuum. *Water Resources Research*, *58*(7). https://doi.org/10.1029/2021wr031275

Grimm, N. B., Gergel, S. E., McDowell, W. H., Boyer, E. W., Dent, C. L., Groffman, P., et al. (2003). Merging aquatic and terrestrial perspectives of nutrient biogeochemistry. *Oecologia*, *137*(4), 485–501. https://doi.org/10.1007/s00442-003-1382-5

Hamamoto, S., Moldrup, P., Kawamoto, K., & Komatsu, T. (2010). Excluded-volume expansion of Archie's law for gas and solute diffusivities and electrical and thermal conductivities in variably saturated porous media. *Water Resources Research*, *46*(6). https://doi.org/10.1029/2009wr008424

Hanson, P. J., Edwards, N. T., Garten, C. T., & Andrews, J. A. (2000). Separating root and soil microbial contributions to soil respiration: A review of methods and observations. *Biogeochemistry*, *48*(1), 115–146. https://doi.org/10.1023/a:1006244819642

Hare, D. K., Helton, A. M., Johnson, Z. C., Lane, J. W., & Briggs, M. A. (2021). Continental-scale analysis of shallow and deep groundwater contributions to streams. *Nature Communications*, *12*(1), 1450. https://doi.org/10.1038/s41467-021-21651-0

Harper, R. J., & Tibbett, M. (2013). The hidden organic carbon in deep mineral soils. *Plant and Soil*, *368*(1–2), 641–648. https://doi.org/10.1007/s11104-013-1600-9

Harrison, H. N., Hammond, J. C., Kampf, S., & Kiewiet, L. (2021). On the hydrological difference between catchments above and below the intermittent-persistent snow transition. *Hydrological Processes*, *35*(11). https://doi.org/10.1002/hyp.14411

Hasenmueller, E. A., Gu, X., Weitzman, J. N., Adams, T. S., Stinchcomb, G. E., Eissenstat, D. M., et al. (2017). Weathering of rock to regolith: The activity of deep roots in bedrock fractures. *Geoderma*, *300*, 11–31. https://doi.org/10.1016/j.geoderma.2017.03.020

Hashimoto, S., Carvalhais, N., Ito, A., Migliavacca, M., Nishina, K., & Reichstein, M. (2015). Global spatiotemporal distribution of soil respiration modeled using a global database. *Biogeosciences*, *12*(13), 4121–4132. https://doi.org/10.5194/bg-12-4121-2015

Hinton, M. J., Schiff, S. L., & English, M. C. (1998). Sources and flowpaths of dissolved organic carbon during storms in two forested watersheds of the Precambrian Shield. *Biogeochemistry*, *41*(2), 175–197. https://doi.org/10.1023/A:1005903428956

Horgby, A., Segatto, P. L., Bertuzzo, E., Lauerwald, R., Lehner, B., Ulseth, A. J., et al. (2019). Unexpected large evasion fluxes of carbon dioxide from turbulent streams draining the world's mountains. *Nature Communications*, *10*(1), 4888. https://doi.org/10.1038/s41467-019-12905-z

Hotchkiss, E. R., Hall Jr, R. O., Sponseller, R. A., Butman, D., Klaminder, J., Laudon, H., et al. (2015). Sources of and processes controlling CO_2 emissions change with the size of streams and rivers. *Nature Geoscience*, *8*(9), 696–699. https://doi.org/10.1038/ngeo2507

Huang, T.-H., Fu, Y.-H., Pan, P.-Y., & Chen, C.-T. A. (2012). Fluvial carbon fluxes in tropical rivers. *Current Opinion in Environmental Sustainability*, *4*(2), 162–169. https://doi.org/10.1016/j.cosust.2012.02.004

Hubbard, S. S., Williams, K. H., Agarwal, D., Banfield, J., Beller, H., Bouskill, N., et al. (2018). The East River, Colorado, watershed: A mountainous community testbed for improving predictive understanding of multiscale hydrological–biogeochemical dynamics. *Vadose Zone Journal*, *17*(1), 1–25. https://doi.org/10.2136/vzj2018.03.0061

Inamdar, S. P., & Mitchell, M. J. (2006). Hydrologic and topographic controls on storm-event exports of dissolved organic carbon (DOC) and nitrate across catchment scales. *Water Resources Research*, *42*(3). https://doi.org/10.1029/2005wr004212

Jencso, K. G., McGlynn, B. L., Gooseff, M. N., Wondzell, S. M., Bencala, K. E., & Marshall, L. A. (2009). Hydrologic connectivity between landscapes and streams: Transferring reach- and plot-scale understanding to the catchment scale. *Water Resources Research*, *45*(4). https://doi.org/10.1029/2008wr007225

Jian, J., Vargas, R., Anderson-Teixeira, K., Stell, E., Herrmann, V., Horn, M., et al. (2021). A restructured and updated global soil respiration database (SRDB-V5). *Earth System Science Data*, *13*(2), 255–267. https://doi.org/10.5194/essd-13-255-2021

Jiang, P., Shuai, P., Sun, A., Mudunuru, M. K., & Chen, X. (2023). Knowledge-informed deep learning for hydrological model calibration: An application to coal Creek watershed in Colorado. *Hydrology and Earth System Sciences*, *27*(14), 2621–2644. https://doi.org/10.5194/hess-27-2621-2023

Johnson, K., Harpold, A., Carroll, R. W. H., Barnard, H., Raleigh, M. S., Segura, C., et al. (2023). Leveraging groundwater dynamics to improve predictions of summer low-flow discharges. *Water Resources Research*, *59*(8). https://doi.org/10.1029/2023wr035126

Johnson, M. S., Weiler, M., Couto, E. G., Riha, S. J., & Lehmann, J. (2007). Storm pulses of dissolved CO_2 in a forested headwater Amazonian stream explored using hydrograph separation. *Water Resources Research*, *43*(11). https://doi.org/10.1029/2007wr006359

Kakalia, Z., Varadharajan, C., Alper, E., Brodie, E. L., Burrus, M., Carroll, R. W. H., et al. (2021). The Colorado East River community observatory data collection. *Hydrological Processes*, *35*(6). https://doi.org/10.1002/hyp.14243

Kaye, J. P., McCulley, R. L., & Burke, I. C. (2005). Carbon fluxes, nitrogen cycling, and soil microbial communities in adjacent urban, native and agricultural ecosystems. *Global Change Biology*, *11*(4), 575–587. https://doi.org/10.1111/j.1365-2486.2005.00921.x

Keller, C. K. (2019). Carbon exports from terrestrial ecosystems: A critical-zone framework. *Ecosystems*, *22*(8), 1691–1705. https://doi.org/10.1007/s10021-019-00375-9

Kerins, D., & Li, L. (2023). High dissolved carbon concentration in arid rocky mountain streams. *Environmental Science & Technology*, *57*(11), 4656–4667. https://doi.org/10.1021/acs.est.2c06675

Kerins, D., Sadayappan, K., Zhi, W., Sullivan, P. L., Williams, K. H., Carroll, R. W. H., et al. (2023). Model_Input_Files_and_Simulation_Output (1.0) [ComputationalNotebook]. https://doi.org/10.5281/zenodo.8247271

Kincaid, D. W., Underwood, K. L., Hamshaw, S. D., Li, L., Seybold, E. C., Stewart, B., et al. (2024). Solute export patterns across the contiguous USA. *Hydrological Processes*, *38*(6), e15197. https://doi.org/10.1002/hyp.15197

Kirchner, J. W. (2009). Catchments as simple dynamical systems: Catchment characterization, rainfall-runoff modeling, and doing hydrology backward. *Water Resources Research*, *45*(2). https://doi.org/10.1029/2008wr006912

Kirschbaum, M. (2006). The temperature dependence of organic-matter decomposition—Still a topic of debate. *Soil Biology and Biochemistry*, *38*(9), 2510–2518. https://doi.org/10.1016/j.soilbio.2006.01.030

Kleber, M., & Johnson, M. G. (2010). Advances in understanding the molecular structure of soil organic matter. *Advances in Agronomy*, *v106*, 77–142. https://doi.org/10.1016/s0065-2113(10)06003-7

Korres, W., Reichenau, T. G., Fiener, P., Koyama, C. N., Bogena, H. R., Cornelissen, T., et al. (2015). Spatio-temporal soil moisture patterns—A meta-analysis using plot to catchment scale data. *Journal of Hydrology*, *520*, 326–341. https://doi.org/10.1016/j.jhydrol.2014.11.042

Leonard, L. T., Vanzin, G. F., Garayburu-Caruso, V. A., Lau, S. S., Beutler, C. A., Newman, A. W., et al. (2022). Disinfection byproducts formed during drinking water treatment reveal an export control point for dissolved organic matter in a subalpine headwater stream. *Water Research*, *15*, 100144. https://doi.org/10.1016/j.wroa.2022.100144

Le Quéré, C., Andrew, R. M., Friedlingstein, P., Sitch, S., Hauck, J., Pongratz, J., et al. (2018). Global carbon budget 2018. *Earth System Science Data*, *10*(4), 2141–2194. https://doi.org/10.5194/essd-10-2141-2018

Li, L. (2019). Watershed reactive transport. *Reviews in Mineralogy and Geochemistry*, *85*(1), 381–418. https://doi.org/10.2138/rmg.2018.85.13

Li, L., Knapp, J. L. A., Lintern, A., Ng, G. H. C., Perdrial, J., Sullivan, P. L., & Zhi, W. (2024). River water quality shaped by land–river connectivity in a changing climate. *Nature Climate Change*, *14*(3), 225–237. https://doi.org/10.1038/s41558-023-01923-x

Li, L., Maher, K., Navarre-Sitchler, A., Druhan, J., Meile, C., Lawrence, C., et al. (2017). Expanding the role of reactive transport models in critical zone processes. *Earth-Science Reviews*, *165*, 280–301. https://doi.org/10.1016/j.earscirev.2016.09.001

Li, L., Sterwart, B., Zhi, W., Sadayappan, K., Ramesh, S., Kerins, D., et al. (2022). Climate controls on river chemistry. *Earth's Future*, *10*(6). https://doi.org/10.1029/2021EF002603

Liu, S., Maavara, T., Brinkerhoff, C. B., & Raymond, P. A. (2022). Global controls on DOC reaction versus export in watersheds: A Damköhler number analysis. *Global Biogeochemical Cycles*, *36*(4). https://doi.org/10.1029/2021gb007278

Lloyd, J., & Taylor, J. A. (1994). On the temperature dependence of soil respiration. *Functional Ecology*, *8*(3), 315–323. https://doi.org/10.2307/2389824

Lukas, J., & Payton, E. (Eds.) (2020). Colorado River Basin climate and hydrology: State of the science. In *Western water Assessment*. University of Colorado.

Maher, K., Steefel, C. I., DePaolo, D. J., & Viani, B. E. (2006). The mineral dissolution rate conundrum: Insights from reactive transport modeling of U isotopes and pore fluid chemistry in marine sediments. *Geochimica et Cosmochimica Acta*, *70*(2), 337–363. https://doi.org/10.1016/j.gca.2005.09.001

Marin-Spiotta, E., Silver, W. L., Swanston, C. W., & Ostertag, R. (2009). Soil organic matter dynamics during 80 years of reforestation of tropical pastures. *Global Change Biology*, *15*(6), 1584–1597. https://doi.org/10.1111/j.1365-2486.2008.01805.x

Markstrom, S. L., Regan, R. S., Hay, L. E., Viger, R. J., Webb, R. M. T., Payn, R. A., & LaFontaine, J. H. (2015). PRMS-IV, the precipitation-runoff modeling system, version 4. In *U.S. Geological Curvey Techniques and methods* (p. 158). https://doi.org/10.3133/tm6B7

Marx, A., Dusek, J., Jankovec, J., Sanda, M., Vogel, T., van Geldern, R., et al. (2017). A review of CO_2 and associated carbon dynamics in headwater streams: A global perspective. *Reviews of Geophysics*, *55*(2), 560–585. https://doi.org/10.1002/2016rg000547

Meingast, K. M., Kane, E. S., Coble, A. A., Marcarelli, A. M., & Toczydlowski, D. (2020). Climate, snowmelt dynamics and atmospheric deposition interact to control dissolved organic carbon export from a northern forest stream over 26 years. *Environmental Research Letters*, *15*(10), 104034. https://doi.org/10.1088/1748-9326/ab9c4e

Meybeck, M., Green, P., & Vörösmarty, C. (2001). A new typology for mountains and other relief classes: An application to global continental water resources and population distribution. *Mountain Research and Development*, *21*(1), 34–45. https://doi.org/10.1659/0276-4741(2001)021[0034:antfma]2.0.co;2

Milly, P. C. D., & Dunne, K. A. (2020). Colorado River flow dwindles as warming-driven loss of reflective snow energizes evaporation. *Science*, *367*, (6483), 1252–1255. https://doi.org/10.1126/science.aay9187

Monod, J. (1949). The growth of bacterial cultures. *Annual Review of Microbiology*, *3*(1), 371–394. https://doi.org/10.1146/annurev.mi.03.100149.002103

Monteith, J. L. (1965). Evaporation and environment. In *Symposia of the Society for experimental biology* (Vol. 19, pp. 205–234).

Musolff, A., Schmidt, C., Selle, B., & Fleckenstein, J. H. (2015). Catchment controls on solute export. *Advances in Water Resources*, *86*, 133–146. https://doi.org/10.1016/j.advwatres.2015.09.026

Neff, J. C., & Asner, G. P. (2001). Dissolved organic carbon in terrestrial ecosystems: Synthesis and a model. *Ecosystems*, *4*(1), 29–48. https://doi.org/10.1007/s100210000058

Newcomer, M., & Rogers, D. B. (2020). Gap-filled meteorological data (2011-2020) and modeled potential evapotranspiration data from the KCOMTCRE2 WeatherUnderground weather station, from the East River Watershed, Colorado [Dataset]. https://doi.org/10.15485/1734790

Overpeck, J. T., & Udall, B. (2020). Climate change and the aridification of North America. *Proceedings of the National Academy of Sciences of the United States of America*, *117*(22), 11856–11858. https://doi.org/10.1073/pnas.2006323117

Peel, M. C., Finlayson, B. L., & McMahon, T. A. (2007). Updated world map of the Köppen-Geiger climate classification. *Hydrology and Earth System Sciences*, *11*(5), 1633–1644. https://doi.org/10.5194/hess-11-1633-2007

Pepin, N., Bradley, R. S., Diaz, H. F., Baraer, M., Caceres, E. B., Forsyth, N., & Yang, D. Q. (2015). Elevation-dependent warming in mountain regions of the world. *Nature Climate Change*, *5*(5), 424–430. https://doi.org/10.1038/nclimate2563

Perdrial, J. N., McIntosh, J., Harpold, A., Brooks, P. D., Zapata-Rios, X., Ray, J., et al. (2014). Stream water carbon controls in seasonally snow-covered mountain catchments: Impact of inter-annual variability of water fluxes, catchment aspect and seasonal processes. *Biogeochemistry*, *118*(1–3), 273–290. https://doi.org/10.1007/s10533-013-9929-y

Pesántez, J., Birkel, C., Gaona, G., Arciniega-Esparza, S., Murray, D. S., Mosquera, G. M., et al. (2023). Spatially distributed tracer-aided modelling to explore DOC dynamics, hot spots and hot moments in a tropical mountain catchment. *Hydrological Processes*, *37*(11). https://doi.org/10.1002/hyp.15020

Pfister, L., Martínez-Carreras, N., Hissler, C., Klaus, J., Carrer, G. E., Stewart, M. K., & McDonnell, J. J. (2017). Bedrock geology controls on catchment storage, mixing, and release: A comparative analysis of 16 nested catchments. *Hydrological Processes*, *31*(10), 1828–1845. https://doi.org/10.1002/hyp.11134

PRISM Climate Group. (2021). *PRISM climate Group*. Oregon State University. Retrieved from https://prism.oregonstate.edu

Raymond, P. A., Hartmann, J., Lauerwald, R., Sobek, S., McDonald, C., Hoover, M., et al. (2013). Global carbon dioxide emissions from inland waters. *Nature*, *503*(7476), 355–359. https://doi.org/10.1038/nature12760

Raymond, P. A., & Saiers, J. E. (2010). Event controlled DOC export from forested watersheds. *Biogeochemistry*, *100*(1–3), 197–209. https://doi.org/10.1007/s10533-010-9416-7

Reynolds, L. L., Lajtha, K., Bowden, R. D., Johnson, B. R., & Bridgham, S. D. (2017). The carbon quality-temperature hypothesis does not consistently predict temperature sensitivity of soil organic matter mineralization in soils from two manipulative ecosystem experiments. *Biogeochemistry*, *136*(3), 249–260. https://doi.org/10.1007/s10533-017-0384-z

Roth, V. N., Dittmar, T., Gaupp, R., & Gleixner, G. (2015). The molecular composition of dissolved organic matter in forest soils as a function of pH and temperature. *PLoS One*, *10*(3), e0119188. https://doi.org/10.1371/journal.pone.0119188

Rumpel, C., & Kögel-Knabner, I. (2011). Deep soil organic matter—A key but poorly understood component of terrestrial C cycle. *Plant and Soil*, *338*(1–2), 143–158. https://doi.org/10.1007/s11104-010-0391-5

Rumsey, C. A., Miller, M. P., Susong, D. D., Tillman, F. D., & Anning, D. W. (2015). Regional scale estimates of baseflow and factors influencing baseflow in the Upper Colorado River Basin. *Journal of Hydrology: Regional Studies*, *4*, 91–107. https://doi.org/10.1016/j.ejrh.2015.04.008

Ryken, A. C., Gochis, D., & Maxwell, R. M. (2022). Unravelling groundwater contributions to evapotranspiration and constraining water fluxes in a high-elevation catchment. *Hydrological Processes*, *36*(1). https://doi.org/10.1002/hyp.14449

Sadayappan, K., Stewart, B., Kerins, D., Vierbicher, A., Zhi, W., Vis, M., et al. (2024a). BioRT-HBV 1.0: A biogeochemical reactive transport model at the watershed scale. *ESS Open Archive*. Preprint. https://doi.org/10.22541/essoar.170561660.04309444/v1

Sadayappan, K., Stewart, B., Kerins, D., Vierbicher, A., Zhi, W., Vis, M. J. P., et al. (2024b). Li-Reactive-Water-Group/BioRT-HBV: V-1.0 BioRT-HBV [Software]. https://doi.org/10.5281/zenodo.10724555

Sadiq, R., & Rodriguez, M. J. (2004). Disinfection by-products (DBPs) in drinking water and predictive models for their occurrence: A review. *Science of the Total Environment*, *321*(1–3), 21–46. https://doi.org/10.1016/j.scitotenv.2003.05.001

Seibert, J., Grabs, T., Kohler, S., Laudon, H., Winterdahl, M., & Bishop, K. (2009). Linking soil- and stream-water chemistry based on a riparian flow-concentration integration model. *Hydrology and Earth System Sciences*, *13*(12), 2287–2297. https://doi.org/10.5194/hess-13-2287-2009

Seibert, J., & Vis, M. J. P. (2012). Teaching hydrological modeling with a user-friendly catchment-runoff-model software package. *Hydrology and Earth System Sciences*, *16*(9), 3315–3325. https://doi.org/10.5194/hess-16-3315-2012

Soulet, G., Hilton, R. G., Garnett, M. H., Dellinger, M., Croissant, T., Ogrič, M., & Klotz, S. (2018). Technical note: In situ measurement of flux and isotopic composition of CO_2 released during oxidative weathering of sedimentary rocks. *Biogeosciences*, *15*(13), 4087–4102. https://doi.org/10.5194/bg-15-4087-2018

Soulsby, C., Piegat, K., Seibert, J., & Tetzlaff, D. (2011). Catchment-scale estimates of flow path partitioning and water storage based on transit time and runoff modelling. *Hydrological Processes*, *25*(25), 3960–3976. https://doi.org/10.1002/hyp.8324

Sprenger, M., Carroll, R. W. H., Dennedy-Frank, J., Siirila-Woodburn, E. R., Newcomer, M. E., Brown, W., et al. (2022). Variability of snow and rainfall partitioning into evapotranspiration and summer runoff across nine mountainous catchments. *Geophysical Research Letters*, *49*(13). https://doi.org/10.1029/2022gl099324

SSURGO. (2023). *Soil survey geographic (SSURGO) database*. Natural Resources Conservation Service, United States Department of Agriculture.

Stewart, B., Shanley, J. B., Kirchner, J. W., Norris, D., Adler, T., Bristol, C., et al. (2022). Streams as mirrors: Reading subsurface water chemistry from stream chemistry. *Water Resources Research*, *58*(1). https://doi.org/10.1029/2021wr029931

Stewart, B., Shanley, J. B., Matt, S., Seybold, E. C., Kincaid, D. W., Vierbicher, A., et al. (2024). Illuminating the "invisible": Substantial deep respiration and lateral export of dissolved carbon from beneath soil. *Water Resources Research*, *60*(6), e2023WR035940. https://doi.org/10.1029/2023WR035940

Stewart, B., Zhi, W., Sadayappan, K., Sterle, G., Harpold, A., & Li, L. (2022). Soil CO_2 controls short-term variation but climate regulates long-term mean of riverine inorganic carbon. *Global Biogeochemical Cycles*, *36*(8), e2022GB007351. https://doi.org/10.1029/2022gb007351

Stielstra, C. M., Lohse, K. A., Chorover, J., McIntosh, J. C., Barron-Gafford, G. A., Perdrial, J. N., et al. (2015). Climatic and landscape influences on soil moisture are primary determinants of soil carbon fluxes in seasonally snow-covered forest ecosystems. *Biogeochemistry*, *123*(3), 447–465. https://doi.org/10.1007/s10533-015-0078-3

Stolze, L., Arora, B., Dwivedi, D., Steefel, C., Li, Z., Carrero, S., et al. (2023). Aerobic respiration controls on shale weathering. *Geochimica et Cosmochimica Acta*, *340*, 172–188. https://doi.org/10.1016/j.gca.2022.11.002

Sullivan, P. L., Stops, M. W., Macpherson, G. L., Li, L., Hirmas, D. R., & Dodds, W. K. (2019). How landscape heterogeneity governs stream water concentration-discharge behavior in carbonate terrains (Konza Prairie, USA). *Chemical Geology*, *527*, 118989. https://doi.org/10.1016/j.chemgeo.2018.12.002

Tang, J., Yurova, A. Y., Schurgers, G., Miller, P. A., Olin, S., Smith, B., et al. (2018). Drivers of dissolved organic carbon export in a subarctic catchment: Importance of microbial decomposition, sorption-desorption, peatland and lateral flow. *Science of the Total Environment*, *622–623*, 260–274. https://doi.org/10.1016/j.scitotenv.2017.11.252

Tank, S. E., Fellman, J. B., Hood, E., & Kritzberg, E. S. (2018). Beyond respiration: Controls on lateral carbon fluxes across the terrestrial-aquatic interface. *Limnology and Oceanography Letters*, *3*(3), 76–88. https://doi.org/10.1002/lol2.10065

Thornton, P. E., Shrestha, R., Thornton, M., Kao, S. C., Wei, Y., & Wilson, B. E. (2021). Gridded daily weather data for North America with comprehensive uncertainty quantification. *Scientific Data*, *8*(1), 190. https://doi.org/10.1038/s41597-021-00973-0

Tobias, C., & Böhlke, J. K. (2011). Biological and geochemical controls on diel dissolved inorganic carbon cycling in a low-order agricultural stream: Implications for reach scales and beyond. *Chemical Geology*. https://doi.org/10.1016/j.chemgeo.2010.12.012

Torres, M. A., & Baronas, J. J. (2021). Modulation of riverine concentration-discharge relationships by changes in the shape of the water transit time distribution. *Global Biogeochemical Cycles*, *35*(1), e2020GB006694. https://doi.org/10.1029/2020GB006694

Tune, A. K., Druhan, J. L., Lawrence, C. R., & Rempe, D. M. (2023). Deep root activity overprints weathering of petrogenic organic carbon in shale. *Earth and Planetary Science Letters*, *607*, 118048. https://doi.org/10.1016/j.epsl.2023.118048

Tune, A. K., Druhan, J. L., Wang, J., Bennett, P. C., & Rempe, D. M. (2020). Carbon dioxide production in bedrock beneath soils substantially contributes to forest carbon cycling. *Journal of Geophysical Research: Biogeosciences*, *125*(12). https://doi.org/10.1029/2020jg005795

U.S. Geological Survey. (2019). The StreamStats program.

Vannote, R. L., Minshall, G. W., Cummins, K. W., Sedell, J. R., & Cushing, C. E. (1980). The river continuum concept. *Canadian Journal of Fisheries and Aquatic Sciences*, *37*(1), 130–137. https://doi.org/10.1139/f80-017

van Vliet, M. T. H., Thorslund, J., Strokal, M., Hofstra, N., Flörke, M., Ehalt Macedo, H., et al. (2023). Global river water quality under climate change and hydroclimatic extremes. *Nature Reviews Earth & Environment*, *4*(10), 687–702. https://doi.org/10.1038/s43017-023-00472-3

Wan, J., Tokunaga, T. K., Dong, W., Williams, K. H., Kim, Y., Conrad, M. E., et al. (2018). Deep unsaturated zone contributions to carbon cycling in semiarid environments. *Journal of Geophysical Research: Biogeosciences*, *123*(9), 3045–3054. https://doi.org/10.1029/2018jg004669

Wang, C., Xie, Y., Liu, S., McCallum, J. L., Li, Q., & Wu, J. (2021). Effects of diffuse groundwater discharge, internal metabolism and carbonate buffering on headwater stream CO2 evasion. *Science of the Total Environment*, *777*, 146230. https://doi.org/10.1016/j.scitotenv.2021.146230

Warner, D. L., Bond-Lamberty, B., Jian, J., Stell, E., & Vargas, R. (2019). Spatial predictions and associated uncertainty of annual soil respiration at the global scale. *Global Biogeochemical Cycles*, *33*(12), 1733–1745. https://doi.org/10.1029/2019gb006264

Weiler, M., & McDonnell, J. J. (2006). Testing nutrient flushing hypotheses at the hillslope scale: A virtual experiment approach. *Journal of Hydrology*, *319*(1–4), 339–356. https://doi.org/10.1016/j.jhydrol.2005.06.040

Wen, H., Li, S. L., Chen, X., Qin, C., & Li, L. (2024). Amplified production and export of dissolved inorganic carbon during hot and wet subtropical monsoon. *Water Resources Research*, *60*(1), e2023WR035292. https://doi.org/10.1029/2023wr035292

Wen, H., Perdrial, J., Abbott, B. W., Bernal, S., Dupas, R., Godsey, S. E., et al. (2020). Temperature controls production but hydrology regulates export of dissolved organic carbon at the catchment scale. *Hydrology and Earth System Sciences*, *24*(2), 945–966. https://doi.org/10.5194/hess-24-945-2020

Wen, H., Sullivan, P. L., Billings, S. A., Ajami, H., Cueva, A., Flores, A., et al. (2022). From soils to streams: Connecting terrestrial carbon transformation, chemical weathering, and solute export across hydrological regimes. *Water Resources Research*, *58*(7). https://doi.org/10.1029/2022wr032314

Wen, H., Sullivan, P. L., Macpherson, G. L., Billings, S. A., & Li, L. (2021). Deepening roots can enhance carbonate weathering by amplifying CO_2-rich recharge. *Biogeosciences*, *18*(1), 55–75. https://doi.org/10.5194/bg-18-55-2021

Weyman, D. R. (1973). Measurements of the downslope flow of water in a soil. *Journal of Hydrology*, *20*(3), 267–288. https://doi.org/10.1016/0022-1694(73)90065-6

Winterdahl, M., Erlandsson, M., Futter, M. N., Weyhenmeyer, G. A., & Bishop, K. (2014). Intra-annual variability of organic carbon concentrations in running waters: Drivers along a climatic gradient. *Global Biogeochemical Cycles*, *28*(4), 451–464. https://doi.org/10.1002/2013gb004770

Winterdahl, M., Laudon, H., Lyon, S. W., Pers, C., & Bishop, K. (2016). Sensitivity of stream dissolved organic carbon to temperature and discharge: Implications of future climates. *Journal of Geophysical Research: Biogeosciences*, *121*(1), 126–144. https://doi.org/10.1002/2015jg002922

Xianwei, S., Sidan, L., Kun, S., Yang, G., & Xuefa, W. (2021). Flux and source of dissolved inorganic carbon in a headwater stream in a subtropical plantation catchment. *Journal of Hydrology*, *600*, 126511. https://doi.org/10.1016/j.jhydrol.2021.126511

Xiao, D., Brantley, S. L., & Li, L. (2021). Vertical connectivity regulates water transit time and chemical weathering at the Hillslope Scale. *Water Resources Research*, *57*(8), e2020WR029207. https://doi.org/10.1029/2020wr029207

Xiao, M., Udall, B., & Lettenmaier, D. P. (2018). On the causes of declining Colorado River streamflows. *Water Resources Research*, *54*(9), 6739–6756. https://doi.org/10.1029/2018wr023153

Xu, Z., Molins, S., Özgen-Xian, I., Dwivedi, D., Svyatsky, D., Moulton, J. D., & Steefel, C. (2022). Understanding the hydrogeochemical response of a mountainous watershed using integrated surface-subsurface flow and reactive transport modeling. *Water Resources Research*, *58*(8). https://doi.org/10.1029/2022wr032075

Yan, Z., Bond-Lamberty, B., Todd-Brown, K. E., Bailey, V. L., Li, S., Liu, C., & Liu, C. (2018). A moisture function of soil heterotrophic respiration that incorporates microscale processes. *Nature Communications*, *9*(1), 2562. https://doi.org/10.1038/s41467-018-04971-6

Zarnetske, J. P., Bouda, M., Abbott, B. W., Saiers, J., & Raymond, P. A. (2018). Generality of hydrologic transport limitation of watershed organic carbon flux across ecoregions of the United States. *Geophysical Research Letters*, *45*(21). https://doi.org/10.1029/2018gl080005

Zeng, X. M., Feng, J., Chen, J., Delgado-Baquerizo, M., Zhang, Q., Zhou, X. Q., et al. (2022). Microbial assemblies associated with temperature sensitivity of soil respiration along an altitudinal gradient. *Science of the Total Environment*, *820*, 153257. https://doi.org/10.1016/j.scitotenv.2022.153257

Zhang, F., Biederman, J. A., Dannenberg, M. P., Yan, D., Reed, S. C., & Smith, W. K. (2021). Five decades of observed daily precipitation reveal longer and more variable drought events across much of the western United States. *Geophysical Research Letters*, *48*(7). https://doi.org/10.1029/2020gl092293

Zhao, L. Y. L., Schulin, R., Weng, L., & Nowack, B. (2007). Coupled mobilization of dissolved organic matter and metals (Cu and Zn) in soil columns. *Geochimica et Cosmochimica Acta*, *71*(14), 3407–3418. https://doi.org/10.1016/j.gca.2007.04.020

Zhi, W., & Li, L. (2020). The shallow and deep hypothesis: Subsurface vertical chemical contrasts shape nitrate export patterns from different land uses. *Environmental Science and Technology*, *54*(19), 11915–11928. https://doi.org/10.1021/acs.est.0c01340

Zhi, W., Li, L., Dong, W., Brown, W., Kaye, J., Steefel, C., & Williams, K. H. (2019). Distinct source water chemistry shapes contrasting concentration-discharge patterns. *Water Resources Research*, *55*(5), 4233–4251. https://doi.org/10.1029/2018wr024257

Zhi, W., Shi, Y., Wen, H., Saberi, L., Ng, G.-H. C., Sadayappan, K., et al. (2022). BioRT-Flux-PIHM v1.0: A biogeochemical reactive transport model at the watershed scale. *Geoscientific Model Development*, *15*(1), 315–333. https://doi.org/10.5194/gmd-15-315-2022

Zhi, W., Williams, K. H., Carroll, R. W. H., Brown, W., Dong, W., Kerins, D., & Li, L. (2020). Significant stream chemistry response to temperature variations in a high-elevation mountain watershed. *Communications Earth & Environment*, *1*(1), 43. https://doi.org/10.1038/s43247-020-00039-w

Zhou, X., Ma, A., Chen, X., Zhang, Q., Guo, X., & Zhuang, G. (2023). Climate warming-driven changes in the molecular composition of soil dissolved organic matter across depth: A case study on the Tibetan Plateau. *Environmental Science and Technology*, *57*(44), 16884–16894. https://doi.org/10.1021/acs.est.3c04899

References From the Supporting Information

Gupta, H. V., Sorooshian, S., & Yapo, P. O. (1998). Toward improved calibration of hydrologic models: Multiple and noncommensurable measures of information. *Water Resources Research*, *34*(4), 751–763. https://doi.org/10.1029/97wr03495

Mai, J. (2023). Ten strategies towards successful calibration of environmental models. *Journal of Hydrology*, *620*, 129414. https://doi.org/10.1016/j.jhydrol.2023.129414

Wagener, T., Boyle, D. P., Lees, M. J., Wheater, H. S., Gupta, H. V., & Sorooshian, S. (2001). A framework for development and application of hydrologic models. *Hydrology and Earth System Sciences*, *5*(1), 13–26. https://doi.org/10.5194/hess-5-13-2001